Structural Applications of Ferritic Stainless Steels

WP 4 Structural Fire Resistance (SCI)

S. Afshan and L. Gardner

Imperial College London

Final Report - June 2013

1. Objectives of the report

Task 4.1 Analysis of isothermal and anisothermal tests presented in Task 4.1 of WP 4
Task 4.2 Preliminary FEM study
Task 4.4 Parametric studies and design recommendations

2. Task 4.1 Isothermal and anisothermal tests (Analysis of results)

The results of isothermal and anisothermal tensile coupon tests, carried out by Outokumpu, presented in Task 4.1, were used to derive strength and stiffness reduction factors for a series of ferritic stainless steel grades. The tested materials were from three different producers, labelled (1), (2) and (3) in this report.

The elevated temperature material properties are expressed as a portion of the corresponding room temperature properties. This leads into the use of strength and stiffness reduction factors for key parameters i.e. the elevated temperature 0.2% proof stress $\sigma_{0.2,\theta}$,ultimate tensile stress $\sigma_{u,\theta,}$ Young's modulus E_θ and the parameter used for determining the strength at 2% total strain, $k_{2,\theta}$. The stiffness reduction factor $k_{E,\theta}$ is defined as the elevated temperature initial tangent modulus E_θ ,normalised by the initial tangent modulus at room temperature E, Eq. (2.1). The strength reduction factor $k_{0.2,\theta}$ is defined as the elevated temperature 0.2% proof stress $\sigma_{0.2,\theta}$, normalised by the room temperature 0.2% proof strength $\sigma_{0.2,}$ Eq. (2.2). The ultimate strength reduction factor $k_{u,\theta}$ is defined as the elevated temperature ultimate tensile stress $\sigma_{u,\theta}$, normalised by the room temperature ultimate tensile stress σ_u, Eq. (2.3). The material strength at 2% total strain $\sigma_{2,\theta}$ is determined in EN 1993-1-2 [1] by a different approach, as described by Eq. (2.4).

$$k_{E,\theta}=\frac{E_\theta}{E} \quad (2.1)$$

$$k_{0.2,\theta}=\frac{\sigma_{0.2,\theta}}{\sigma_{0.2}} \quad (2.2)$$

$$k_{u,\theta}=\frac{\sigma_{u,\theta}}{\sigma_u} \quad (2.3)$$

$$\sigma_{2,\theta}=\sigma_{0.2,\theta}+k_{2,\theta}\,(\sigma_{u,\theta}-\sigma_{0.2,\theta}) \quad (2.4)$$

Anisothermal tensile coupon tests on ferritic stainless steel grades EN 1.4509 and 1.4521 were carried out. Reduction factors $k_{0.2,\theta}$, $k_{u,\theta}$ and $k_{2,\theta}$, based on the anisothermal tests, were determined by Outokumpu and these values were taken for the analysis herein. A series of isothermal tests on ferritic stainless steel grades EN 1.4003, 1.4016, 1.4509, 1.4521 and 1.4621 were also performed. Strain control was used to perform the isothermal tensile coupon tests, with the strain rate changing from 0.005 min^{-1}, at typically 1.0% strain, to 0.2 min^{-1} until fracture. The change in the test rate resulted in a step in the measured stress-strain curve, giving higher stress values for the stress at 2% total strain and the ultimate tensile stress than those obtained if the lower strain rate was continued. It is well known that strain rate has a marked effect on the measured material behaviour at elevated temperature. Therefore, material properties used for modelling and design of structures in fire should be determined in such way that is representative of that observed in real fire situations. On the basis of using the stress at 2% total strain for fire design and assuming 60 min fire resistance, the approximate expected strain rate experienced by a structural member in fire is 0.00033 min^{-1}. Hence, the measured stress-strain curves were adjusted appropriately, by extrapolating the

low strain rate part 0.005 min^{-1}, as it provides a better representation of the real fire situations, but, following the actual shape of the measured stress-strain curve. The adjusted stress-strain curves were used to determine reduction factors $k_{0.2,\theta}$, $k_{u,\theta}$, $k_{E,\theta}$ and $k_{2,\theta}$. For each temperature, two tests were carried out, the results of which were averaged for obtaining the final values.

Stiffness reduction factors were based on the isothermal test results whereas a combination of both the isothermal test results and the anisothermal test results were used for all other reduction factors. Owing to the difficulties associated with determining accurate Young's modulus values at both room temperature and elevated temperatures, it is proposed that a common single set of stiffness reduction factors be used for all ferritic stainless steel grades. Figure 2.1 shows the test results for the Young's modulus at elevated temperature with the mean fit line through the data points. The proposed reduction factor curve, which is a smoothed version of the mean fit line, along with the EN 1993-1-2 values for both steel and stainless steel are also depicted.

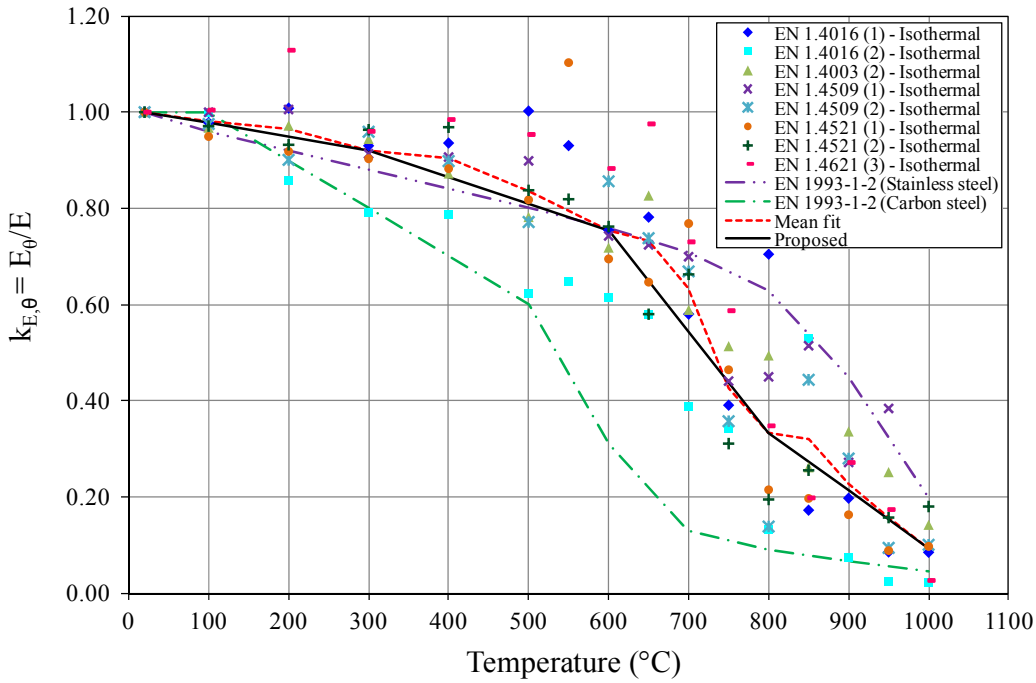

Fig. 2.1. Proposed Young's modulus reduction factors for all ferritic stainless steel grades

From examining all the test results, it was observed that ferritic stainless steel grades may be divided into two groups on the basis of their similar elevated temperature properties, as illustrated in Figures 2.2 and 2.3 for the 0.2% proof stress and the ultimate tensile stress reduction factors. Ferritic stainless steel grades EN 1.4509, 1.4521 and 1.4621, referred to as group I, have similar elevated temperature properties and at high temperatures – exceeding 550 °C – are superior to the EN 1.4003 and 1.4016 grades, referred to as group II. This approach was also recommended by Outokumpu. At higher temperatures, above 600 °C, the stress-strain response of ferritic stainless steels becomes almost elastic, perfectly plastic. This results in high values for the $k_{2,\theta}$ parameter used for calculating the stress at 2% total strain. In order to ensure that the stress at 2% total strain values are safe for design, the $k_{2,\theta}$ parameter has been set to 0.5 for temperatures above 600 °C.

Figures 2.4-2.6 show the test results for the $k_{0.2,\theta}$, $k_{u,\theta}$ and $k_{2,\theta}$, respectively for group I. Figures 2.7-2.9 show the test results for the $k_{0.2,\theta}$, $k_{u,\theta}$ and $k_{2,\theta}$, respectively for group II. In each case, the mean fit line through the data points and the final proposed curve which is a smoothed version of the mean fit line is also provided. A summary of the proposed values is provided in Tables 2.1 and 2.2.

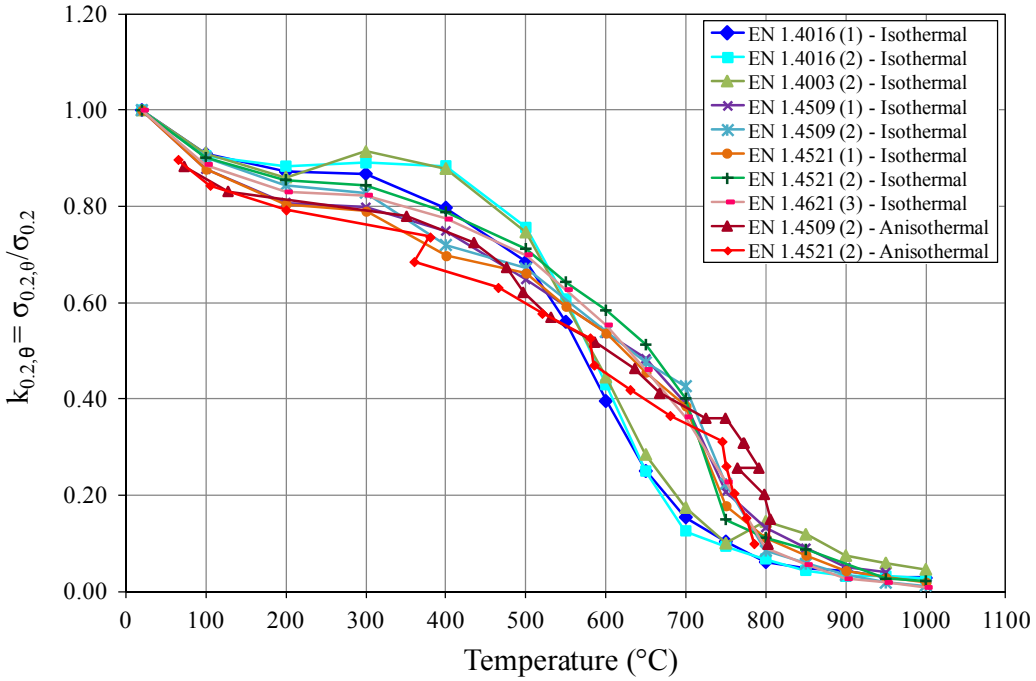

Fig.2.2. Comparison of the $k_{0.2,\theta}$ reduction factor for tested ferritic stainless steel grades

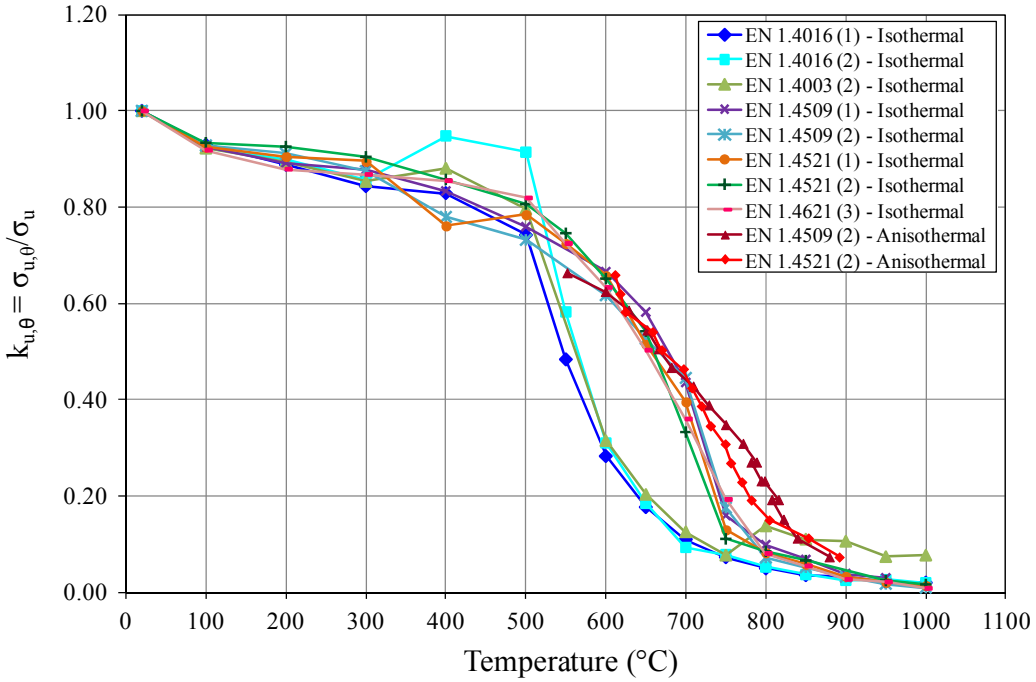

Fig.2.3. Comparison of the $k_{u,\theta}$ reduction factor for tested ferritic stainless steel grades

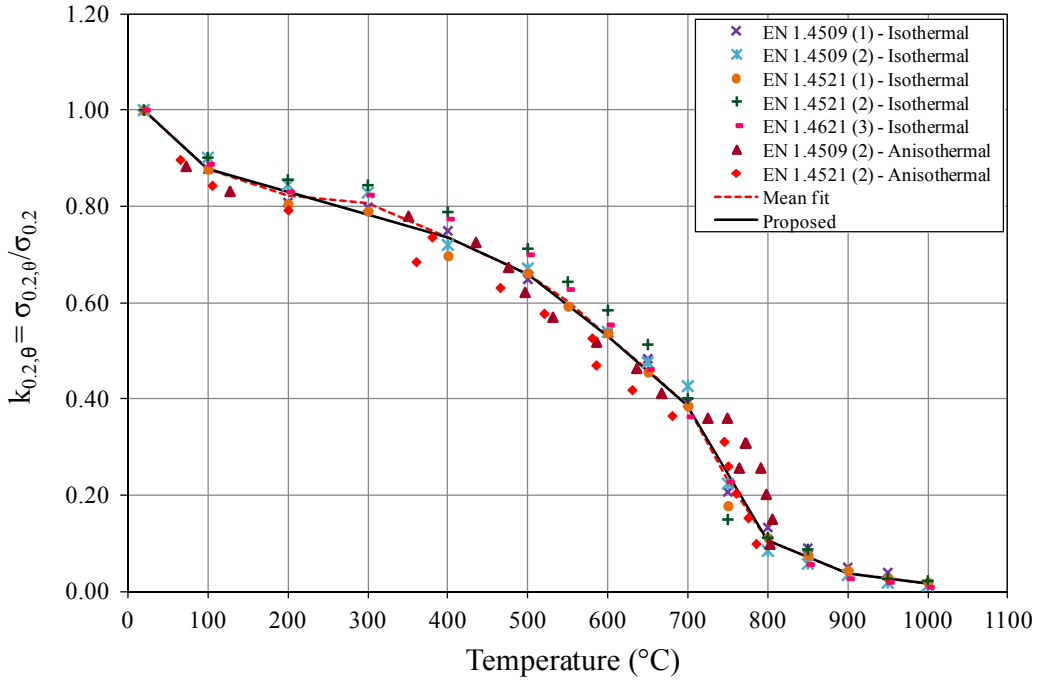

Fig. 2.4. Proposed 0.2% proof stress reduction factors for group I grades

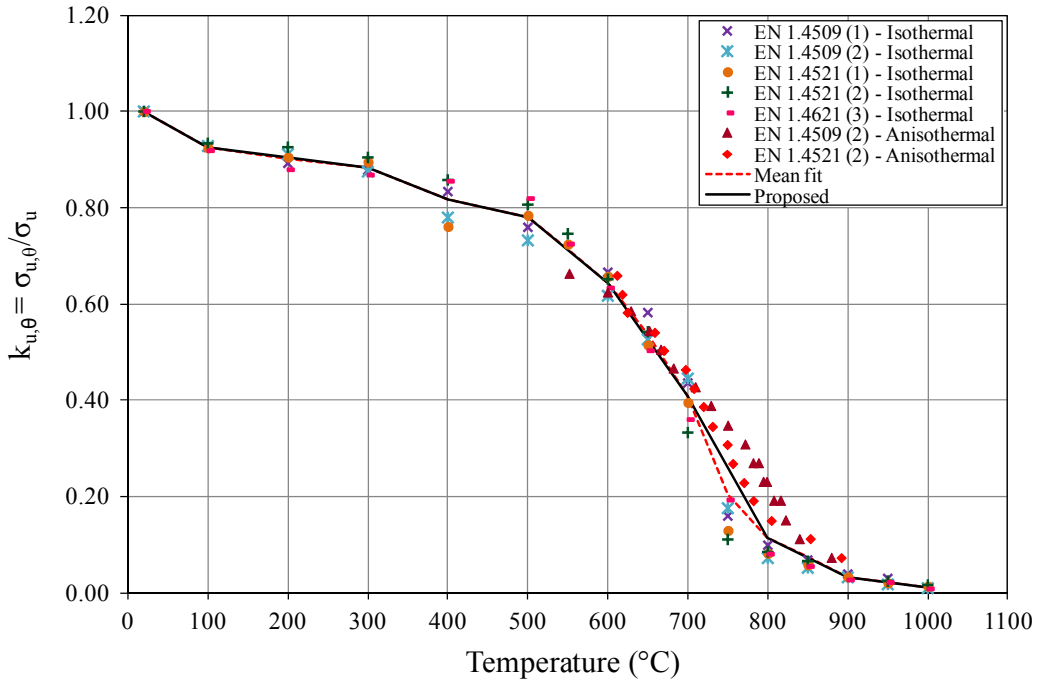

Fig. 2.5. Proposed ultimate tensile stress reduction factors for group I grades

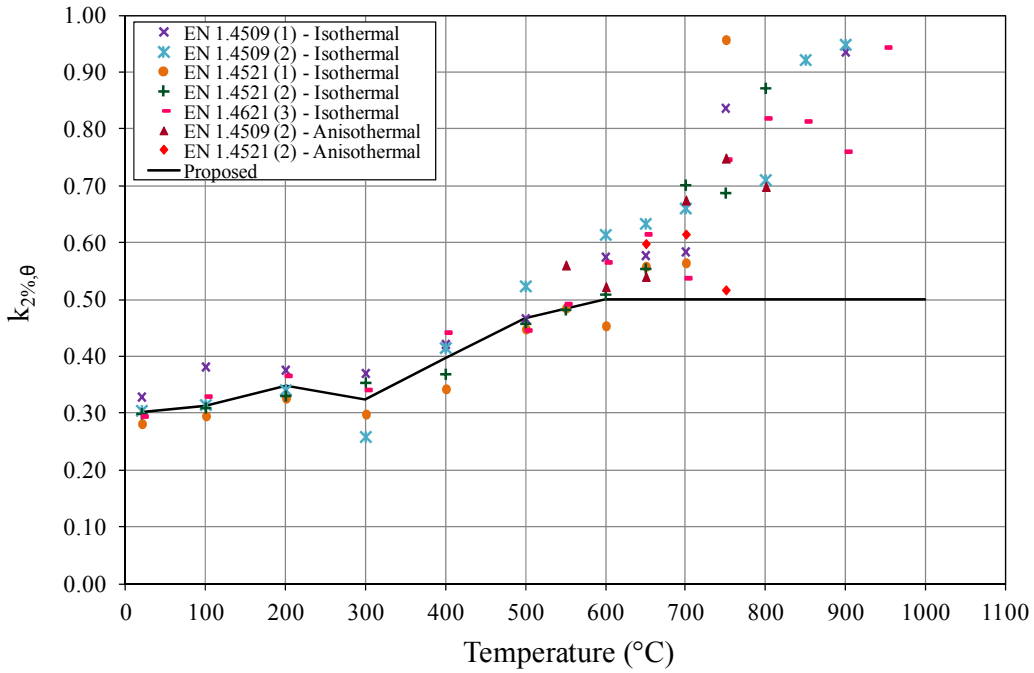

Fig. 2.6. Proposed $k_{2,\theta}$ factors for group I grades

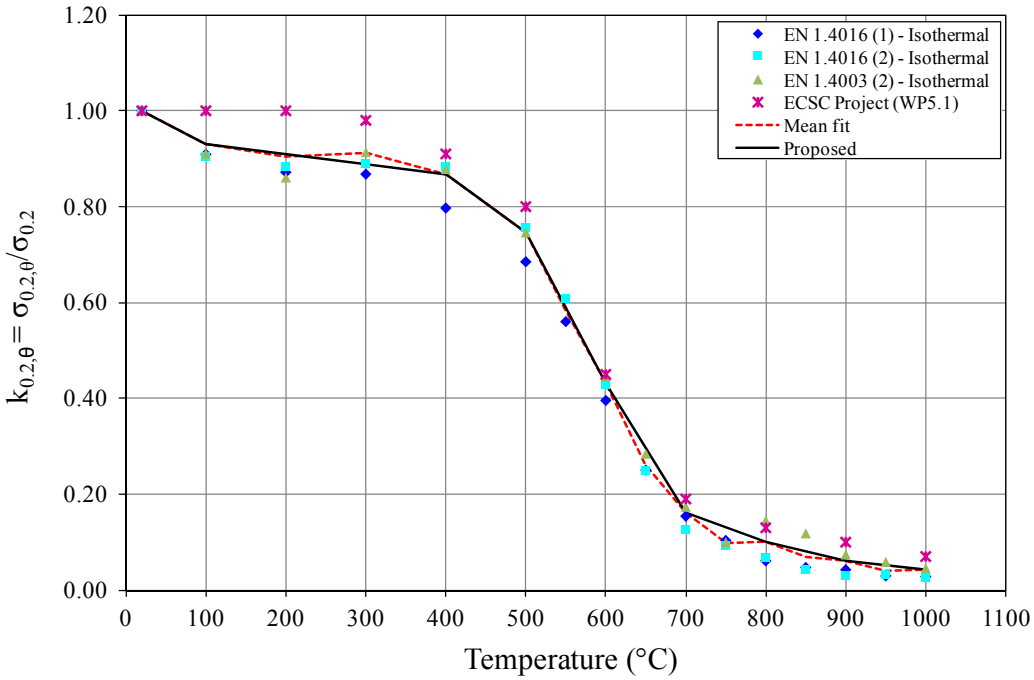

Fig. 2.7. Proposed 0.2% proof stress reduction factors for group II grades

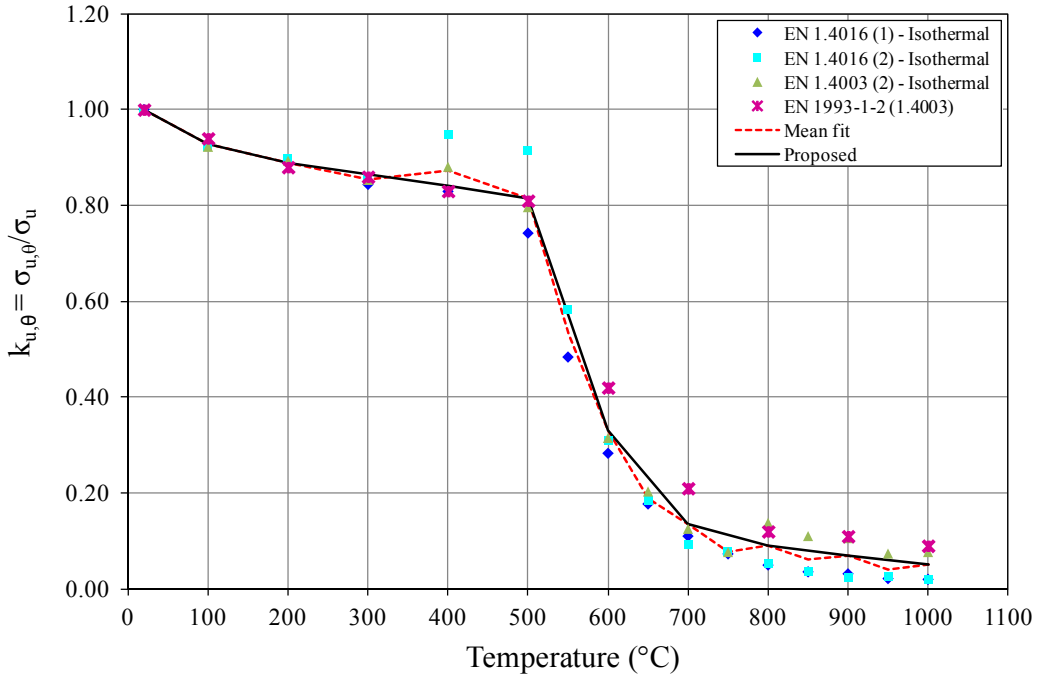

Fig. 2.8. Proposed ultimate tensile stress reduction factors for group II grades

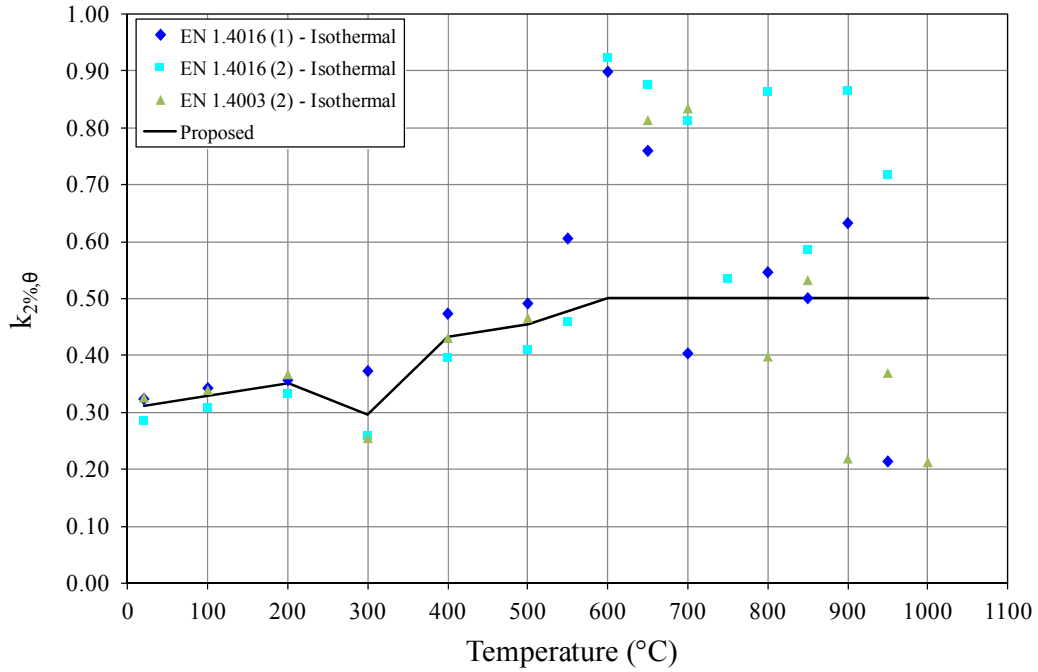

Fig. 2.9. Proposed $k_{2,\theta}$ factors for group II grades

Table 2.1. Proposed reduction factors for group I ferritic stainless steel grades (EN 1.4509, 1.4521 and 1.4621)

Temperature (°C)	$k_{E,\theta}$	$k_{0.2,\theta}$	$k_{u,\theta}$	$k_{2.0,\theta}$
20	1.00	1.00	1.00	0.30
100	0.98	0.88	0.93	0.31
200	0.95	0.83	0.91	0.35
300	0.92	0.78	0.88	0.32
400	0.86	0.73	0.82	0.40
500	0.81	0.66	0.78	0.47
600	0.75	0.53	0.64	0.50
700	0.54	0.39	0.41	0.50
800	0.33	0.10	0.11	0.50
900	0.21	0.04	0.03	0.50
1000	0.09	0.02	0.01	0.50

Table 2.2. Proposed reduction factors for group II ferritic stainless steel grades (EN 1.4003 and 1.4016)

Temperature (°C)	$k_{E,\theta}$	$k_{0.2,\theta}$	$k_{u,\theta}$	$k_{2.0,\theta}$
20	1.00	1.00	1.00	0.31
100	0.98	0.93	0.93	0.33
200	0.95	0.91	0.89	0.35
300	0.92	0.89	0.87	0.30
400	0.86	0.87	0.84	0.43
500	0.81	0.75	0.82	0.46
600	0.75	0.43	0.33	0.50
700	0.54	0.16	0.13	0.50
800	0.33	0.10	0.09	0.50
900	0.21	0.06	0.07	0.50
1000	0.09	0.04	0.05	0.50

3. Task 4.2 & 4.4 Preliminary FE study, parametric study and design recommendations

3.1. Introductions

The aim of this section is to develop and validate numerical models for predicting the resistance of ferritic stainless steel beams and columns in fire, leading into the results of parametric studies, appraisal of current design guidance and proposals for suitable design recommendations.

3.2. Validation of Numerical models

3.2.1 Column tests

The results of the fire tests on three EN 1.4003 columns from Task 4.3, combined with a series of column fire test results from the literature on austenitic (EN 1.4301) stainless steel columns from [2, 3] were used for the validation of the finite element models. A summary of these tests, including nominal section size, boundary conditions, applied loads and critical

temperature, are provided in Tables 1-3. All column buckling tests were performed on square hollow sections (SHS) and rectangular hollow section (RHS) specimens. The RHS columns, given in Table 1, were formed by welding two press-braked channel sections tip-to-tip along the length of the column. The manufacturing process of the SHS columns and beams, given in Tables 2 and 3, involved cold-rolling into a circular tube followed by sizing into the final cross-section geometry. All fire tests were performed anisothermally, whereby the load was applied at room temperature and was maintained at a constant level while the temperature was increased until failure.

Table 3.1. Summary of austenitic column tests reported in [2]

Nominal section size	Boundary conditions	Applied load (kN)	Critical specimen temperature (°C)
RHS 150×100×6	Fixed	268	801
RHS 150×75×6	Fixed	140	883
RHS 100×75×6	Fixed	156	806

Table 3.2. Summary of austenitic column tests reported in [3]

Nominal section size	Boundary conditions	Applied load (kN)	Critical specimen temperature (°C)
SHS 40×40×4 (T1)	Pinned	45	872
SHS 40×40×4 (T2)	Pinned	129	579
SHS 40×40×4 (T3)	Pinned	114	649
SHS 40×40×4 (T4)	Pinned	95	710
SHS 40×40×4 (T5)	Pinned	55	832
SHS 40×40×4 (T7)	Pinned	75	766

Table 3.3. Summary of ferritic column tests reported in Task 4.3

Nominal section size	Boundary conditions	Applied load (kN)	Critical furnace temperature (°C)	Failure time (min)
SHS 80×80×3-3000mm	Fixed	72	709.4	12 min 9 sec
SHS 80×80×3-2500 mm	Fixed	78	707.7	12 min 0 sec
RHS 120×80×3-2500 mm	Fixed	100	705.0	11 min 51 sec

3.2.2 Beam tests

The results of the two fire tests on EN 1.4509 beams from Task 4.3 were used for the validation of the finite element models. Both beams, one uncoated and one coated with fire protection, were loaded in four point bending configuration. A summary of these tests, including nominal section size, boundary conditions, applied loads and critical temperature, are provided in Table 3.4.

Table 3.4. Summary of ferritic beam tests reported in Task 4.3

Nominal section size	Boundary conditions	Total Applied load (kN)	Max specimen temperature (°C)	Failure time (min)
SHS 80×40×2 - uncoated	Pinned	9.96	791	24
SHS 80×40×2 - coated	Pinned	9.96	833	57

3.2.3 General modelling description

The non-linear finite element analysis package ABAQUS, Version 6.10-1 [4] was used to replicate the elevated temperature response of stainless steel column and beam tests. A sequentially coupled thermal-stress analysis was carried out where three types of numerical analyses were performed for each model – a linear elastic buckling analysis to determine the buckling mode shapes, and a heat transfer analysis to obtain the temperature development in the structural members, were initially carried out. The results were subsequently incorporated into a geometrically and materially non-linear stress analysis. The non-linear stress analysis was performed in two steps to simulate the anisothermal loading condition of the column and beam fire tests. In the first step, the load was applied to the structure at room temperature. This load was maintained at a constant level during the second step while the evolution of the temperature with the fire exposure time was applied. For the case of the austenitic stainless steel columns and ferritic beams, the steel surface temperature was measured during the test and was directly imported into the models.

Shell elements were adopted to simulate the stainless steel tubular hollow section columns and beams as is customary for modelling of thin-walled structures. The four-node doubly curved general-purpose shell element with reduced integration S4R, for the structural model, and D4S, for the thermal model, which has performed well in numerous similar applications (e.g. [5] and [6]) were used. A suitable mesh size, providing accurate results with practical computational times, with a minimum of ten elements across each plate was adopted. The test boundary conditions were replicated by restraining suitable displacement and rotation degrees of freedom at the columns and beams ends. Measured geometric dimensions were used in each model to replicate the corresponding test behaviour.

3.2.4 Elevated temperature material stress-strain modelling

The performance of finite element models is highly sensitive to the prescribed material parameters, hence making an accurate representation of the material characteristics essential. For the ferritic stainless steel column and beam tests, the modified compound Ramberg-Osgood material model for elevated temperatures provided in [7], along with the measured elevated temperature reduction factors for the EN 1.4003 and EN 1.4509 grades, respectively (presented in Task 4.1) and the measured room temperature material properties were used. The room temperature material properties for the flat faces of the tested sections were obtained from the results reported in Task 4.3. As for the corner regions, for the ferritic column, corner material properties of the same length of tubes as the fire tests were measured as part of a parallel testing programme and were used herein. For the beam tests, where no corner coupon tests were conducted, the predictive model in [8] was used to determine the room temperature 0.2% proof strength of the corner regions. For the case of the literature column tests, the measured material stress-strain curves at elevated temperatures were utilised in the development of the finite element models.

The corner strength enhancement was confined to the corner region for the press-braked sections, while for the cold-rolled sections, a uniform strength enhancement for the corner region plus an extension of 2t, where t is the material thickness, beyond the corner radius into the flat faces of the section was used as specified in [9]. It has been shown that the beneficial effect of cold-work is lost at high temperatures of about 800 ^{o}C and above [3, 10]. Hence, in order to allow for this in the numerical models, the corner regions were assigned the same material properties as the flat faces for temperatures above 800 ^{o}C.

ABAQUS requires that the material properties are specified in terms of true stress σ_{true} and log plastic strain ε_{ln}^{p}, which may be derived from the nominal engineering stress–strain curves as defined in Eqs. (1) and (2), respectively, where σ_{nom} and ε_{nom} are engineering stress and strain, respectively and E is the Young's modulus.

$$\sigma_{true} = \sigma_{nom}(1 + \varepsilon_{nom}) \quad (3.1)$$

$$\varepsilon_{ln}^{p} = \ln(1 + \varepsilon_{nom}) - \frac{\sigma_{true}}{E} \quad (3.2)$$

3.2.5 Thermal properties

For austenitic stainless steel, the thermal properties from EN 1993-1-2 [1] were incorporated in the models. The thermal properties of ferritic stainless steels are different from the austenitic stainless steels and are not currently covered in EN 1993-1-2 [1]. For the EN 1.4003 grade, thermal expansion data were sourced from EN 10088-1 [11] and specific heat and thermal conductivity data were obtained from the StahlDat SX database [12] . For the EN 1.4509 grade, thermal expansion data were sourced from manufacturer's product data sheet from Aperam [13] and specific heat and thermal conductivity data were obtained from the StahlDat SX [12] database for similar ferritic stainless steel grade EN 1.4521.

3.2.6 Initial geometric imperfections

Initial geometric imperfections are introduced into structural sections during production, fabrication and handling and can significantly influence structural behaviour. Imperfection shapes of the form of the lowest global and local buckling modes obtained from a linear elastic eigenvalue buckling analysis were utilized. A global imperfection amplitude of L/2000, where L is the column total length, was adopted for the austenitic stainless steel columns, while the test measured imperfection amplitudes were used for the ferritic stainless steel columns. The measured local imperfection amplitude was used for the beams while for the columns, the amplitude w_0 predicted by the Dawson and Walker model as adapted for stainless steel [14], given by Eq. (3.3) was used, where t is the plate thickness, $\sigma_{0.2}$ is the material 0.2% proof stress and σ_{cr} is the plate critical elastic buckling stress.

$$w_0 = 0.023\, t\, (\sigma_{0.2}/\sigma_{cr}) \quad (3.3)$$

3.2.7 Residual stresses

Through thickness bending residual stresses are introduced in cold-formed sections through plastic deformations induced during the production process. Such residual stresses have been

observed previously [15, 16] and it was concluded by Ashraf et al. [14] that provided the coupons were not straightened prior to testing, the residual stresses would be inherently present in the material stress-strain curve and do not therefore have to be explicitly included in numerical models. Membrane residual stresses which may be introduced due to differential cooling following welding of the stainless steel tubular sections, have been found to have an insignificant effect on the performance of FE models. Hence, residual stresses were not included in the FE models.

3.2.8 Heat transfer model

The heat transfer model was used to obtain the temperature distribution in the stainless steel members during the fire exposure time. For the beam tests, thermocouples attached to the surface of the specimens were used to measure the steel temperature during the test. Hence, the thermal model was only used to replicate the temperature distribution for the unprotected tested beam specimen, providing a validated modelling procedure for the subsequent parametric studies. For the ferritic column tests, the specimen temperature was not measured during the tests and the furnace temperature was measured only. Hence, the thermal model was used to obtain the evolution of specimen temperature with the fire exposure time for the columns, which is required for the stress analysis part of the modelling procedure. Combined convection and radiation heat transfer mechanisms were used to model the heat transfer from the surrounding air to the exposed surface of the specimens while conduction heat transfer mechanism was used to model the heat transfer within the structural members. For the columns, the measured furnace temperature was applied uniformly to the specimens' surface with a uniform initial temperature of 20 °C. Since the beam top flange and the beam ends were not exposed to fire directly, the measured furnace temperature was applied to the exposed surfaces only, resulting in a temperature gradient both within the cross-section and along the length of the beam. The convective heat transfer coefficient and the emissivity factor were taken as 25 W/m^2K and 0.4, respectively, as specified in EN 1993-1-2 [1].

3.2.9 Validation results

The results of the thermal analysis model and the structural analysis for both the columns and the beams are presented in this section. Figures 3.1-3.4 show the time-temperature results obtained from the thermal analysis model for the three ferritic columns and the unprotected steel beam.

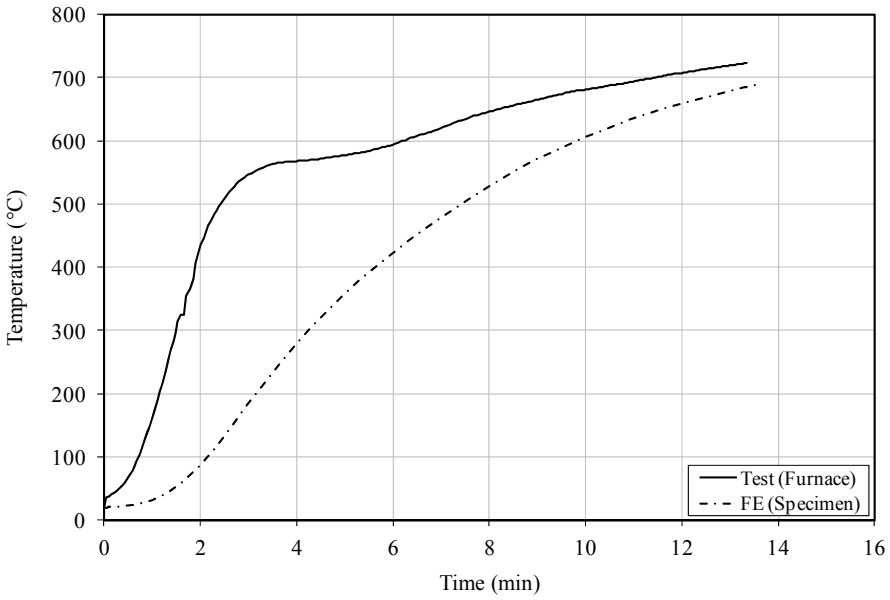

Fig. 3.1 FE Temperature development in SHS 80×80×3 (L=3000 mm)

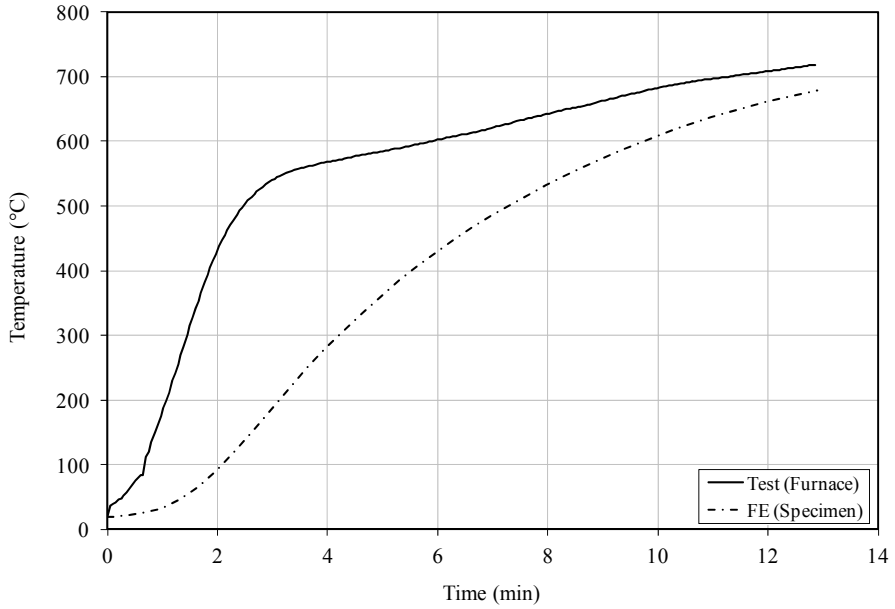

Fig. 3.2 FE Temperature development in SHS 80×80×3 (L=2500 mm)

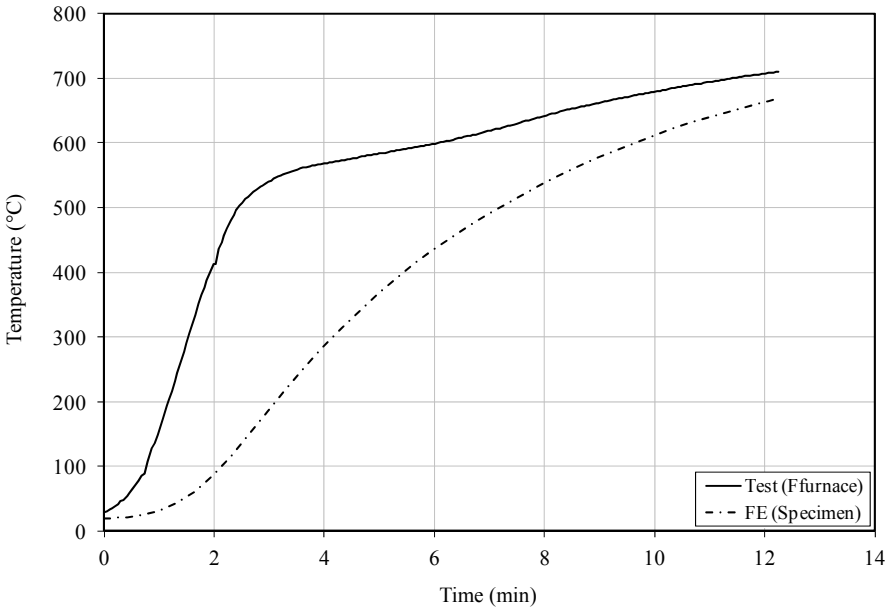

Fig. 3.3 FE Temperature development in RHS 120×80×3 (L=2500 mm)

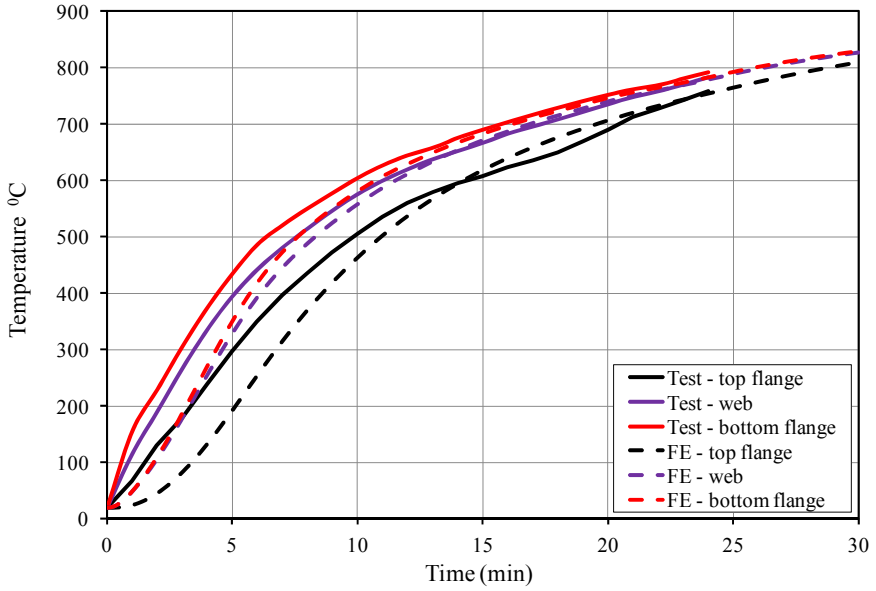

Fig. 3.4 FE Temperature development in SHS 80×80×2 beam

A total of nine austenitic stainless steel columns, three ferritic stainless steel columns and two ferritic stainless steel beams were modelled using the sequentially coupled thermal-stress analysis procedure. The fire performance criteria set out in EN 1363-1 [17] for vertically loaded members and flexural loaded elements were used to determine the critical failure temperature of the columns. It states that a column is deemed to have failed when both the vertical contraction and the rate of vertical contraction have exceeded L/100 mm and 3L/1000 mm/min, respectively, where L is initial column height in mm, were used to determine the critical failure temperature of the columns. Similarly, for beams, the limiting

deflection and the limiting rate of deflection are $L^2/400d$ mm and $L^2/9000d$ mm/min, respectively, where L is the clear span of the test specimen and d is the distance from the compressive fibre to the tensile fibre in the section.

Figures 3.5-3.8 compare the test results with the FE results for the ferritic beam and column tests. A summary of the comparison between the test and FE results is provided in Table 3.5. For the austenitic stainless steel columns, the FE models give a mean FE/test critical temperature of 0.90 and a coefficient of variation of 0.03, and provide safe-side predictions of the fire resistance of the test column specimens. This under-prediction may be due to the application of uniform temperature through the thickness of the column section. In addition, all column tests were partially protected near the column ends to prevent the effect of sudden temperature variation at the start of the test, leaving a smaller exposed length than the full length used in the FE simulations. For the ferritic stainless steel beams and columns, the FE and test results are in very good agreement with a mean FE/Test critical temperature of 1.004 and a coefficient of variation of 0.018. From the comparison of the test and FE results, it is concluded that the described FE models are capable of safely replicating the non-linear, large deflection response of the stainless steel beams and columns in fire.

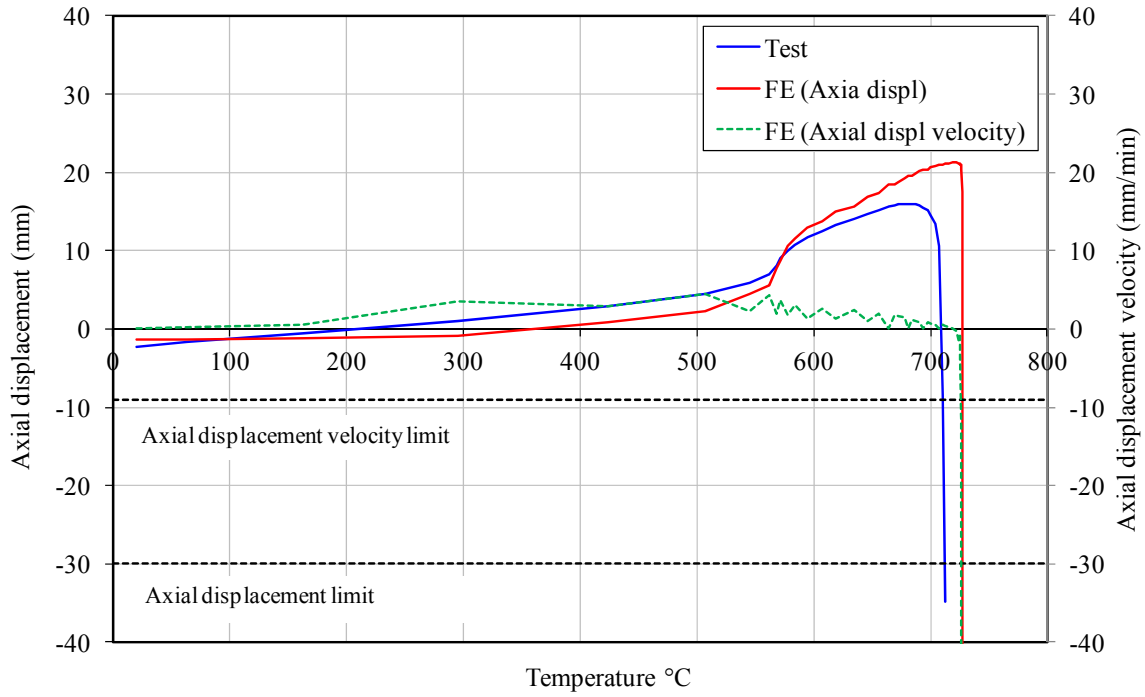

Fig. 3.5. Vertical displacement versus temperature for the SHS 80×80×3 -3000 mm specimen.

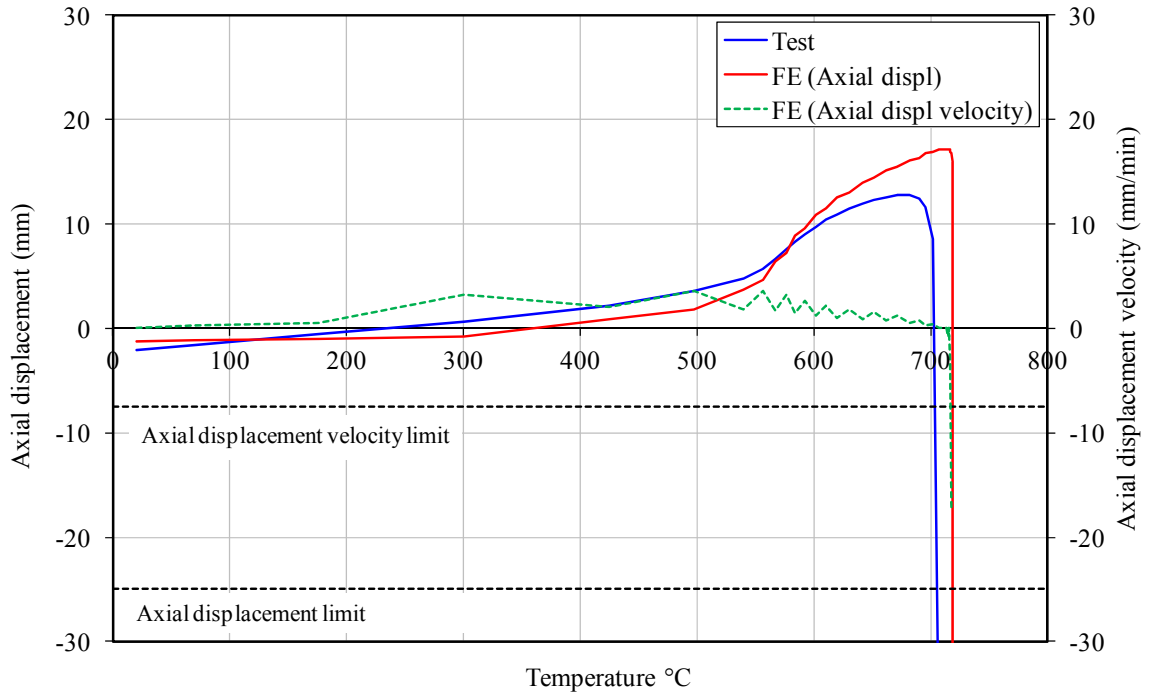

Fig. 3.6. Vertical displacement versus temperature for the SHS 80×80×3 – 2500 mm specimen.

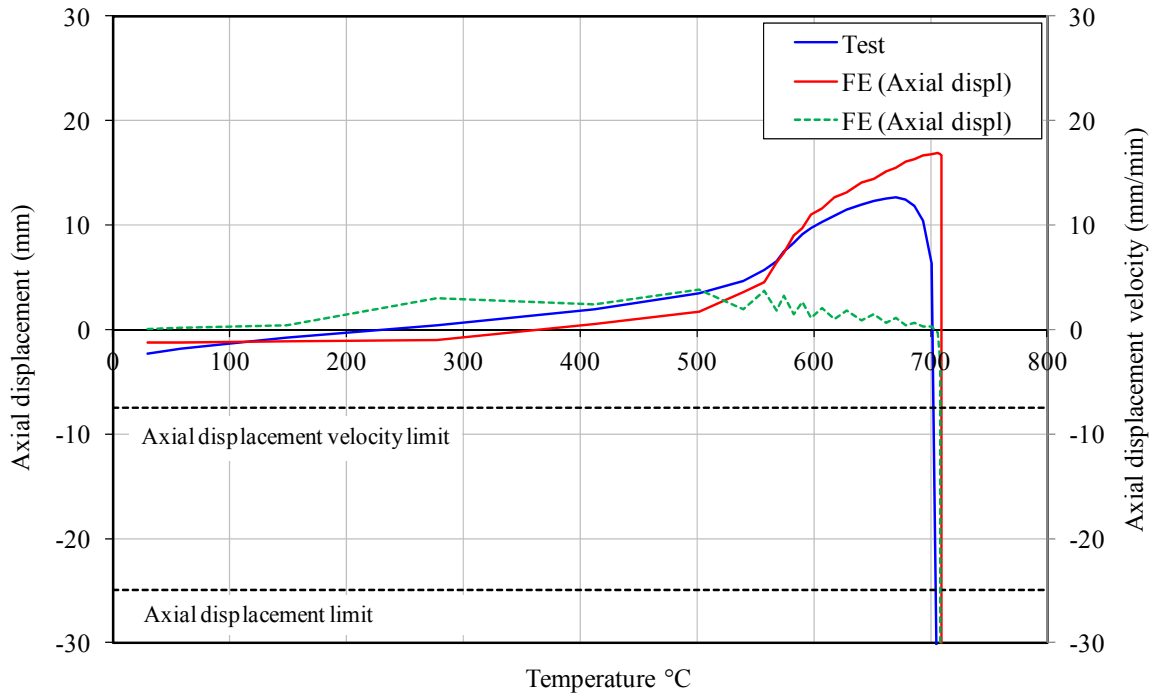

Fig. 3.7. Vertical displacement versus temperature for the RHS 120×80×3 – 2500 mm specimen.

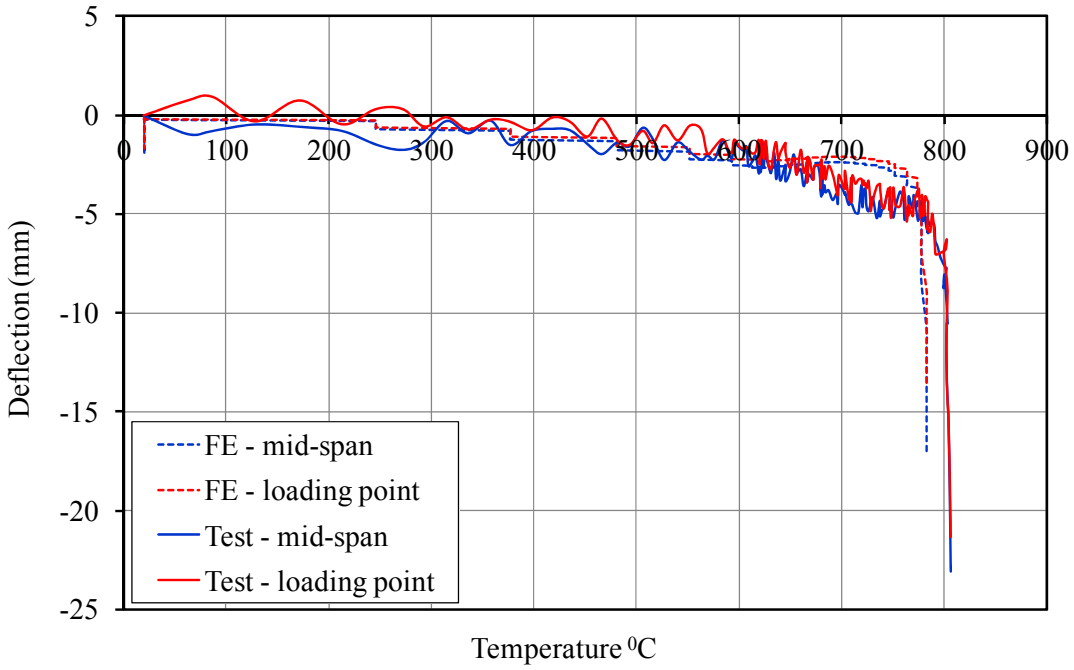

Fig. 3.8. Deflection versus temperature for the SHS 80×40×2 uncoated beam specimen.

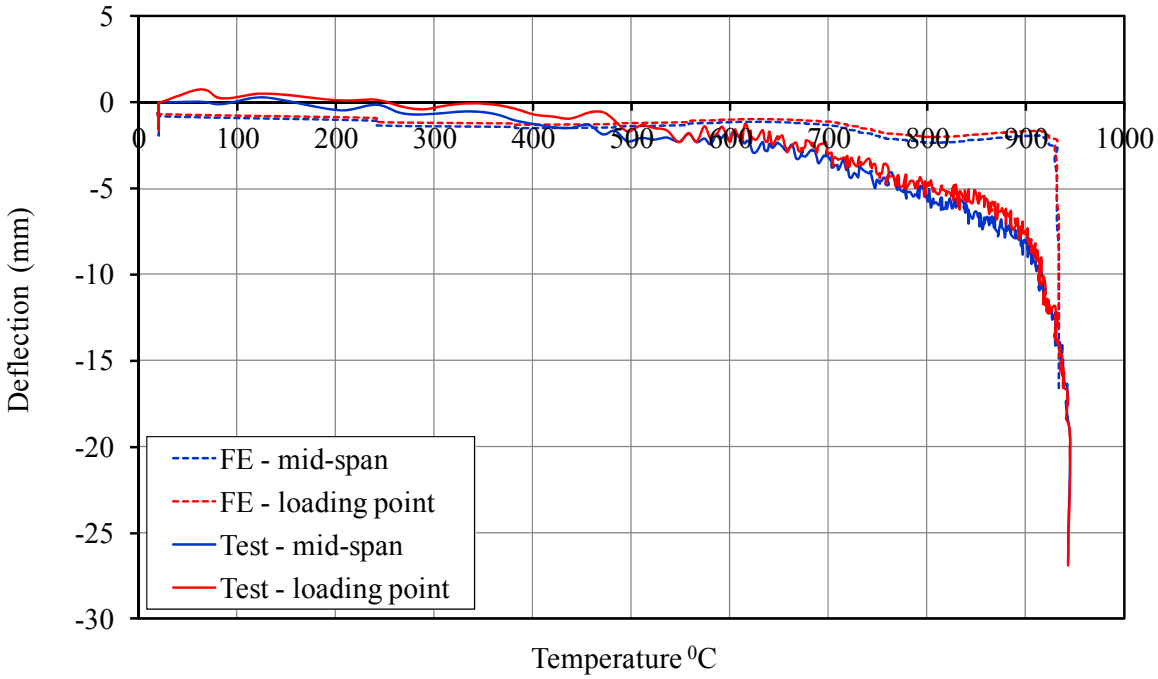

Fig. 3.9. Deflection versus temperature for the SHS 80×40×2 coated beam specimen.

Table 3.5. Comparison of critical temperatures between test and FE results

Nominal section size	Critical temperature (°C)		
	Test	FE	FE/Test
RHS 150×100×6	801	757	0.91
RHS 150×75×6	883	814	0.92
RHS 100×75×6	806	744	0.92
SHS 40×40×4 (1)	872	750	0.86
SHS 40×40×4 (2)	579	502	0.87
SHS 40×40×4 (3)	649	608	0.94
SHS 40×40×4 (4)	710	646	0.91
SHS 40×40×4 (5)	832	722	0.87
SHS 40×40×4 (7)	766	681	0.89
SHS 80×80×3-3000	709	726	1.02
SHS 80×80×3-2500	708	718	1.02
RHS 120×80×3-2500	705	709	1.01
SHS 80×40×2-coated	803	783	0.98
SHS 80×40×2-uncoated	944	934	0.99

3.3 Parametric studies and results

Having validated the FE models, a series of parametric studies was performed. The same modelling procedures as explained in the previous sections were employed for the parametric study models. The standard temperature-time curve given in [18] was used for the thermal model and anisothermal loading condition was used for the structural model.

3.3.1 Columns

Parametric studies were used to investigate the influence of variation of cross-section slenderness, member slenderness and applied load level on the fire performance of ferritic stainless steel columns.

Three section sizes, namely SHS 80×80×6, RHS 120×80×6 and SHS 80×80×3 were employed to study the buckling response of ferritic stainless steel columns. The elevated temperature material properties pertaining to ferritic stainless steel grade EN 1.4003, group I, were used. The global imperfection amplitude was taken as L/1000, where L is the column length, in accordance with the permitted out-of-straightness tolerance in EN 1090-2 [19]. The local imperfection amplitude was taken as that predicted by Eq. (3.3). All columns were pin-ended at both ends. Due to the symmetry in the geometry and the boundary conditions of the analyzed specimens, only half of the section, but over the full length, was modelled. The column lengths were varied from 0.5 m to 3.0 m and provided a range of room temperature member slenderness of 0.25-1.55. Three different load levels were applied to each column specimen: 25%, 45% and 65% of the room temperature minor axis buckling resistance, determined in accordance with EN 1993-1-4 [20].

The obtained results are shown in Figures 3.8-3.10 for the SHS 80×80×6, RHS 120×80×6 and SHS 80×80×3 cross-sections, respectively. As anticipated, the column failure temperature reduces with increased load level. The variation of critical temperature with load level is also dependent on the member slenderness. This is expected as the member

slenderness is dependent on the material strength and stiffness and its degradation with temperature.

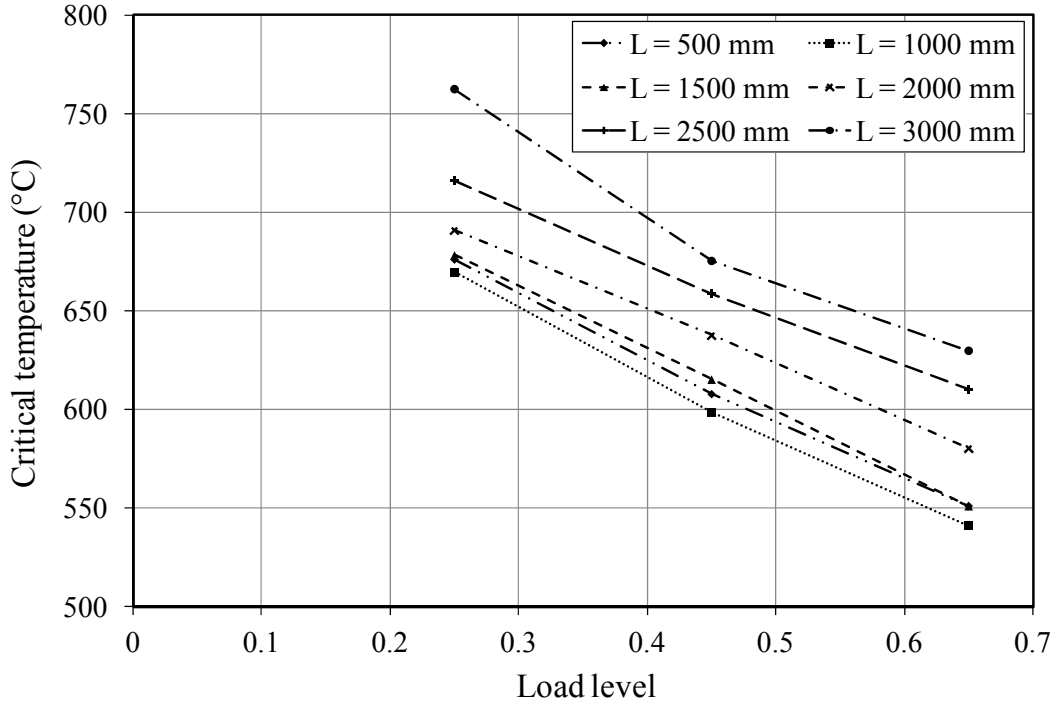

Fig. 3.8. Effect of load level on the RHS 120×80×6 column critical temperature.

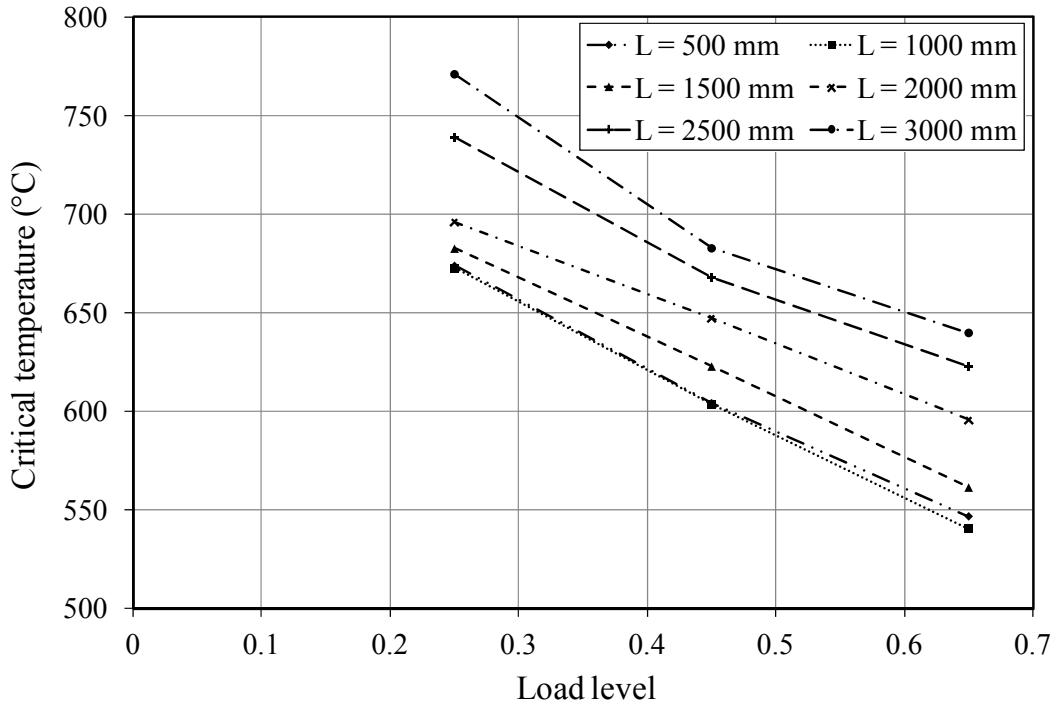

Fig. 3.9. Effect of load level on the SHS 80×80×6 column critical temperature.

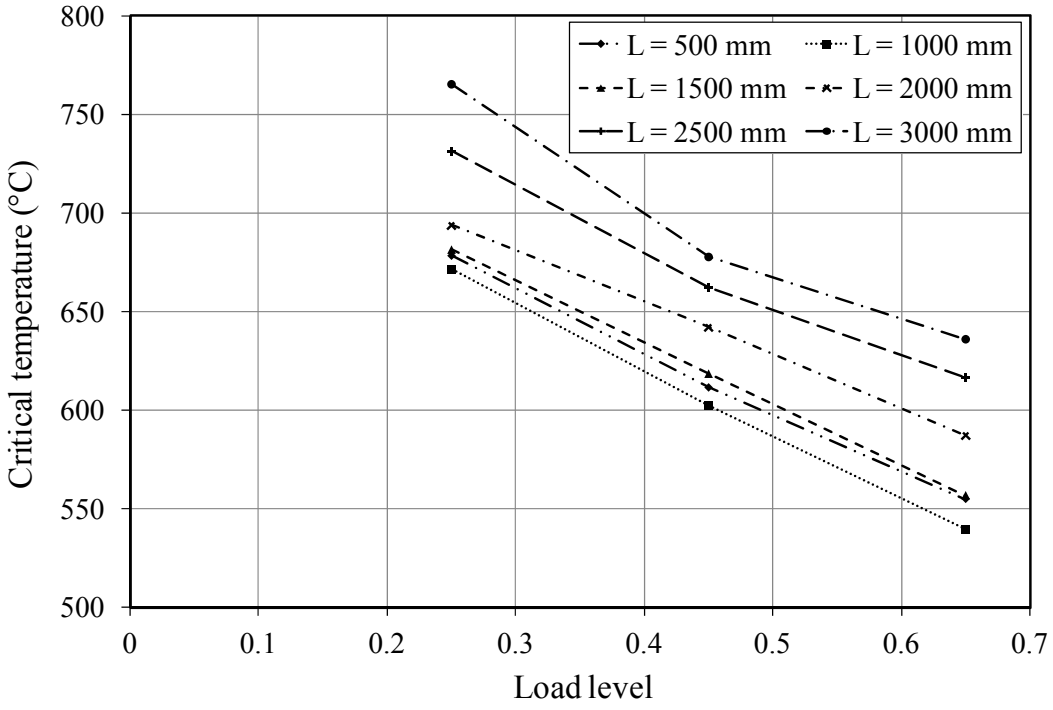

Fig. 3.10. Effect of load level on the SHS 80×80×3 column critical temperature.

The effect of cross-section slenderness on the fire resistance of ferritic stainless steel columns was carried out by varying the cross-section thickness, while maintaining the cross-section outer dimensions, column length and the load level. The local imperfection amplitude was taken as that predicted by Eq. (3.3). The cross-section slenderness was taken as the plate slenderness $\bar{\lambda}_p$ defined in EN 1993-1-4 [20]. The cross-section width and depth were both taken as 80 mm, the length was taken as 500 mm, ensuring stub column behaviour with no global buckling, and the thicknesses were 1.0, 1.25, 1.50, 1.75, 2.0, 2.25, 2.5, 3.0, 3.5, 4.0, 4.5, 5.0 and 6.0 mm, providing a range of plate slenderness values $\bar{\lambda}_p$= 0.24 - 2.05. Material properties pertaining to both group I, EN 1.4509, and group II, EN 1.4003, ferritic grades were employed. The applied load level was taken as 20% of the room temperature cross-section compression resistance from EN 1993-1-4 [20]. The obtained results are shown in Figure 3.11. As anticipated, the column failure temperature reduces with increased cross-section plate slenderness. The enhanced fire performance of group I ferritic grades, at temperatures above 550 °C, is also evident, where higher failure temperatures are obtained.

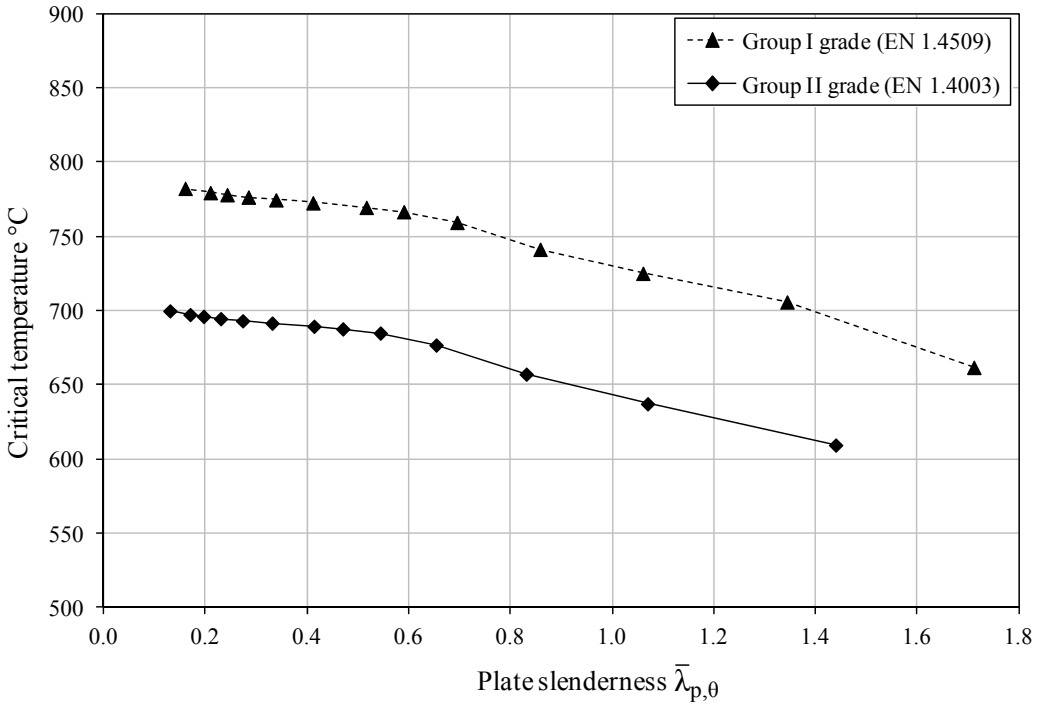

Fig. 3.11. Effect of cross-section slenderness on the critical temperature.

3.3.2 Beams

Parametric studies were conducted to study the influence of cross-section slenderness and load level on the performance of ferritic stainless steel beams. All components were modelled as 900 mm long simply supported beams loaded in 4-point bending configuration at third points. In all models advantage of the symmetry in geometry, boundary conditions and load was exploited by modelling one quarter of the specimen and applying suitable boundary conditions. The SHS 80×40 with a total of six different thicknesses, 1.5, 2.0, 2.5, 3.0, 4.0 and 5.0 mm, were used to obtain a range of section slenderness values. For each of the six cross-sections considered, six load ratios were also considered, ranging from 0.2 to 0.7 at intervals of 0.1. The load levels were based on numerically obtained failure loads at room temperature. The obtained results are shown in Figure 3.12 and show that the beam failure temperature reduces with increased load level and also depends on the cross-section thickness.

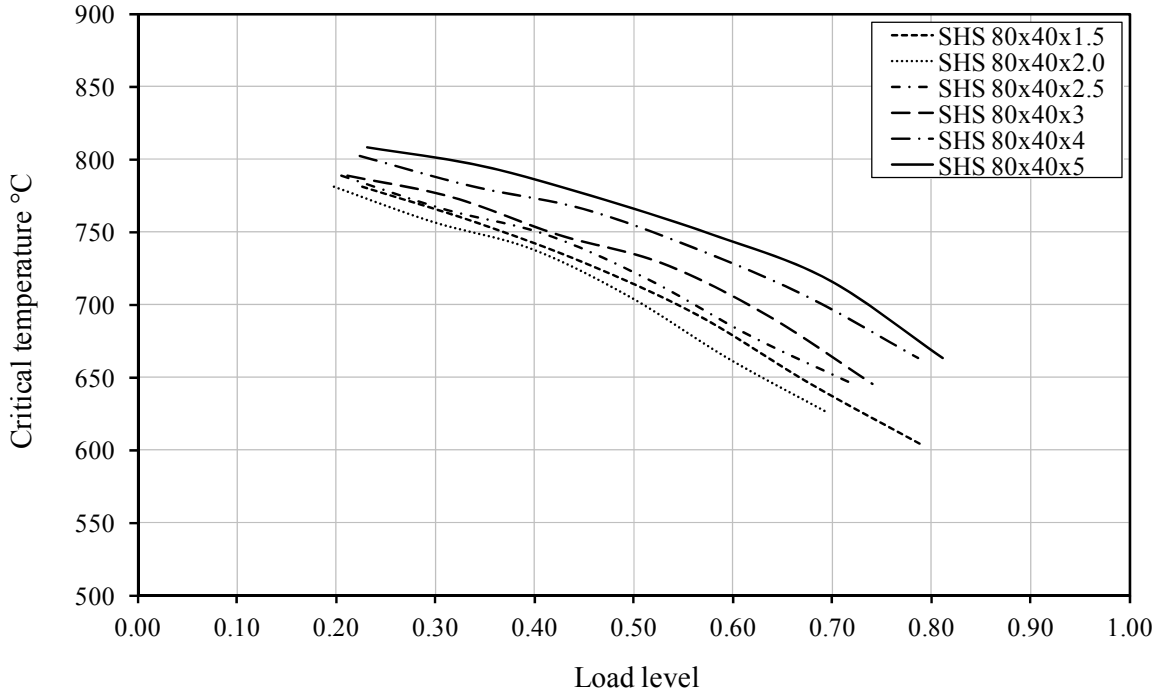

Fig. 3.12. Effect of cross-section slenderness and load level on the critical temperature

3.4 Design recommendations

This section presents a comparison of the parametric study results and the test results for both the beams and the columns with the existing design rules provided in EN 1993-1-2 [1] and its modified versions. Amendments to the current design procedures, in line with the obtained results, are proposed.

3.4.1 Material strength for design

In determining the structural fire resistance of stainless steel members, the characteristic material strength parameters provided in Table 3.6 are recommended in existing design guidance and proposals made in the literature. More rationalised design strength parameters are proposed, as summarised in Table 3.7 and are justified herein. Since the design at member level is mainly controlled by material stiffness, which reduces significantly beyond the 0.2% proof stress point, the elevated temperature design yield stress $f_{y,\theta}$ is recommended to be taken as the elevated temperature 0.2% proof stress, given as the product of the strength reduction factor based on 0.2% plastic strain, $k_{0.2,\theta}$ and the design yield stress at 20°C, $\sigma_{0.2}$. At cross-section level, relatively large strain levels could be reached before the onset of local buckling for the case of Class 1 and 2 cross-sections. Hence, the stress at 2% total strain may be utilised in determining the cross-section resistance of Class 1 and 2 sections, as is currently recommended in EN 1993-1-2 [1]. The stress at 2% total strain is also used for the design of Class 3 cross-sections in EN 1993-1-2 [1]. This is considered inappropriate as local buckling is expected before this strain level is reached and moreover, the spread of plasticity through the section in reaching the 2% strain limit is not in accordance with the linear stress distribution assumed for Class 3 sections in bending.

Table 3.6: Elevated temperature design strength parameters from current design guidance

Design standard	Columns	Beams
EN 1993-1-4 & EN 1993-1-2. [1, 20]	Cross-section design: $f_{y,\theta}=\sigma_{2,\theta}$ for Class 1,2 and 3 $f_{y,\theta}=\sigma_{0.2,\theta}$ for Class 4 Member design: $f_{y,\theta}=\sigma_{2,\theta}$ for Class 1,2 and 3 $f_{y,\theta}=\sigma_{0.2,\theta}$ for Class 4	Cross-section design: $f_{y,\theta}=\sigma_{2,\theta}$ for Class 1,2 and 3 $f_{y,\theta}=\sigma_{0.2,\theta}$ for Class 4 Member design: $f_{y,\theta}=\sigma_{2,\theta}$ for Class 1,2 and 3 $f_{y,\theta}=\sigma_{\theta,0.2}$ for Class 4
Euro Inox/SCI Design Manual. [21]	Cross-section design: $f_{y,\theta}=\sigma_{0.2,\theta}$ for all Classes Member design: $f_{y,\theta}=\sigma_{0.2,\theta}$ for all Classes	Cross-section design: $f_{y,\theta}=\sigma_{2,\theta}$ for Class 1,2 and 3 $f_{y,\theta}=\sigma_{0.2,\theta}$ for Class 4 Member design: $f_{y,\theta}=\sigma_{0.2,\theta}$ for Classes
Ng and Gardner. [5]	Cross-section design: $f_{y,\theta}=\sigma_{2,\theta}$ for Class 1 and 2 $f_{y,\theta}=\sigma_{0.2,\theta}$ for Class 3 and 4 Member design: $f_{y,\theta}=\sigma_{2,\theta}$ for Class 1 and 2 $f_{y,\theta}=\sigma_{0.2,\theta}$ for Class 3 and 4	Cross-section design: $f_{y,\theta}=\sigma_{2,\theta}$ for Class 1 and 2 $f_{y,\theta}=\sigma_{0.2,\theta}$ for Class 3 and 4 Member design: $f_{y,\theta}=\sigma_{2,\theta}$ for Class 1 and 2 $f_{y,\theta}=\sigma_{0.2,\theta}$ for Class 3 and 4
Lopes et al. [22]	As in EN 1993-1-2 & EN 1993-1-4	As in EN 1993-1-2 & EN 1993-1-4
Uppfeldt et al. [23]	As in Ng and Gardner (2007)	As in Ng and Gardner (2007)

Table 3.7. Proposed elevated temperature design strength parameters

Columns	Beams
Cross-section design: $f_{y,\theta}=\sigma_{2,\theta}$ for Class 1 and 2 $f_{y,\theta}=\sigma_{0.2,\theta}$ for Class 3 and 4	Cross-section design: $f_{y,\theta}=\sigma_{2,\theta}$ for Class 1 and 2 $f_{y,\theta}=\sigma_{0.2,\theta}$ for Class 3 and 4
Member design: $f_{y,\theta}=\sigma_{0.2,\theta}$ for all Classes	Member design: $f_{y,\theta}=\sigma_{0.2,\theta}$ for all Classes

3.4.2 Local buckling treatment

In classifying cross-sections at room temperature, the material factor ε, given in Eq. (3.4) for stainless steel, is used to allow for variation in material yield strength f_y and stiffness E as provided in EN 1993-1-4 [20]. A similar definition is employed for carbon steel in EN 1993-1-1 [24], taking E as 210000 N/mm^2, resulting in Eq. (3.5). Since in fire, the rate of degradation of material strength and stiffness does not occur at the same rate, this material strength parameter becomes temperature dependent. EN 1993-1-2 [1] uses a factor of 0.85 in

the definition of the material strength parameter at elevated temperatures while the Euro Inox/SCI Design Manual for Stainless Steel [21] adopts the room temperature definition.

$$\varepsilon = \left(\frac{235}{f_y}\frac{E}{210000}\right)^{0.5} \tag{3.4}$$

$$\varepsilon = \left(\frac{235}{f_y}\right)^{0.5} \tag{3.5}$$

Annex E of EN 1993-1-2 [1] recommends that for the case of class 4 sections, the effective cross-section area and the effective section modulus be determined in accordance with EN 1993-1-4 [20], i.e. based on the material properties at 20°C. Hence, the definition of plate slenderness at room temperature is not modified for elevated temperatures design, which is not consistent with the adopted cross-section classification approach and also does not allow for the elevated temperature effects. It was proposed by Ng and Gardner [5] and later by Upffeldt et al. [23] that the true variation of stiffness to strength ratio with temperature should be employed in treatment of local buckling at elevated temperatures, including the cross-section classification and the determination of the effective section properties, leading to the definition of the elevated temperature material parameter ε_θ. Table 3.8 provides a summary of the current design guidance and proposals for the treatment of local buckling in fire design of stainless steel sections.

A series of more relaxed new cross-section classification limits for the room temperature design of stainless steel structures were proposed by Gardner and Theofanous [25] which were derived and statistically validated based on all relevant published test data on stainless steel at room temperature. For consistency with the new Class 3 to Class 4 limit, a modified version of the EN 1993-1-4 [20] effective width formula was also proposed. The suitability of these proposals for the design of ferritic stainless steel structures at elevated temperatures is assessed herein.

Figure 3.13 shows the FE results with the effective width formulae provided in EN 1993-1-4 and its modified version given by Gardner and Theofanous (2008), as presented in Eqs. (3.6)-(3.8), respectively. The effective width equation provided in EN 1993-1-5 [26] is also shown.

$$\rho = \frac{0.772}{\bar{\lambda}} - \frac{0.125}{\bar{\lambda}^2} \tag{3.6}$$

$$\rho = \frac{0.772}{\bar{\lambda}} - \frac{0.079}{\bar{\lambda}^2} \tag{3.7}$$

$$\rho = \frac{1}{\bar{\lambda}} - \frac{0.22}{\bar{\lambda}^2} \tag{3.8}$$

Both, the EN 1993-1-4 [20] effective width equation and its modified version by Theofanous and Gardner [25] provide good predictions of the FE results, with the latter slightly over-predicting the results at intermediate plate slenderness range. However, it is proposed that in determining the cross-section resistance of ferritic stainless steel structures at elevated temperatures, the cross-section classification limits and the effective width equation from Gardner and Theofanous [25] in conjunction with the temperature dependent material

parameter ε_θ as in [5] and [23], be employed. A summary of the recommended design method is provided in Table 3.9. Note that the notation $k_{2,\theta}$ in Tables 3.8 and 3.9 refers to the ratio of the elevated temperature stress at 2% total strain to the room temperature 0.2% proof stress.

Table 3.8. Elevated temperature cross-section design approaches from current design guidance

Design standard	Cross-section classification limits	Effective width formula
EN 1993-1-4 & EN 1993-1-2. [1, 20]	EN 1993-1-4 limits with $\varepsilon_\theta = 0.85\sqrt{235/f_y}$ All cross-section classes	EN 1993-1-4 formula
Euro Inox/SCI Design Manual. [21]	EN 1993-1-4 limits with $\varepsilon_\theta = \left[(235/f_y)(E/210000)\right]^{0.5}$ All cross-section classes	EN 1993-1-4 formula
Ng and Gardner. [5]	EN 1993-1-4 limits with $\varepsilon_\theta = \left[\left(\frac{235}{f_y}\frac{E}{210000}\right)\left(\frac{k_{E,\theta}}{k_{2,\theta}}\right)\right]^{0.5}$ Class 1&2 sections at room temperature $\varepsilon_\theta = \left[\left(\frac{235}{f_y}\frac{E}{210000}\right)\left(\frac{k_{E,\theta}}{k_{0.2,\theta}}\right)\right]^{0.5}$ Class 3&4 sections at room temperature	EN 1993-1-4 formula with $\bar{\lambda}_{p,\theta} = \frac{\bar{b}/t}{28.4\varepsilon_\theta\sqrt{k_\sigma}}$
Lopes et al. [22]	As in EN 1993-1-2 & EN 1993-1-4	As in EN 1993-1-2 & EN 1993-1-4
Uppfeldt et al. [23]	EN 1993-1-4 limits with $\varepsilon_\theta = \left[\left(\frac{235}{f_y}\frac{E}{210000}\right)\left(\frac{k_{E,\theta}}{k_{2,\theta}}\right)\right]^{0.5}$ Class 1 & 2 sections at room temperature $\varepsilon_\theta = \left[\left(\frac{235}{f_y}\frac{E}{210000}\right)\left(\frac{k_{E,\theta}}{k_{0.2,\theta}}\right)\right]^{0.5}$ Class 3 & 4 sections at room temperature	EN 1993-1-4 formula with $\bar{\lambda}_{p,\theta} = \frac{\bar{b}/t}{28.4\varepsilon_\theta\sqrt{k_\sigma}}$

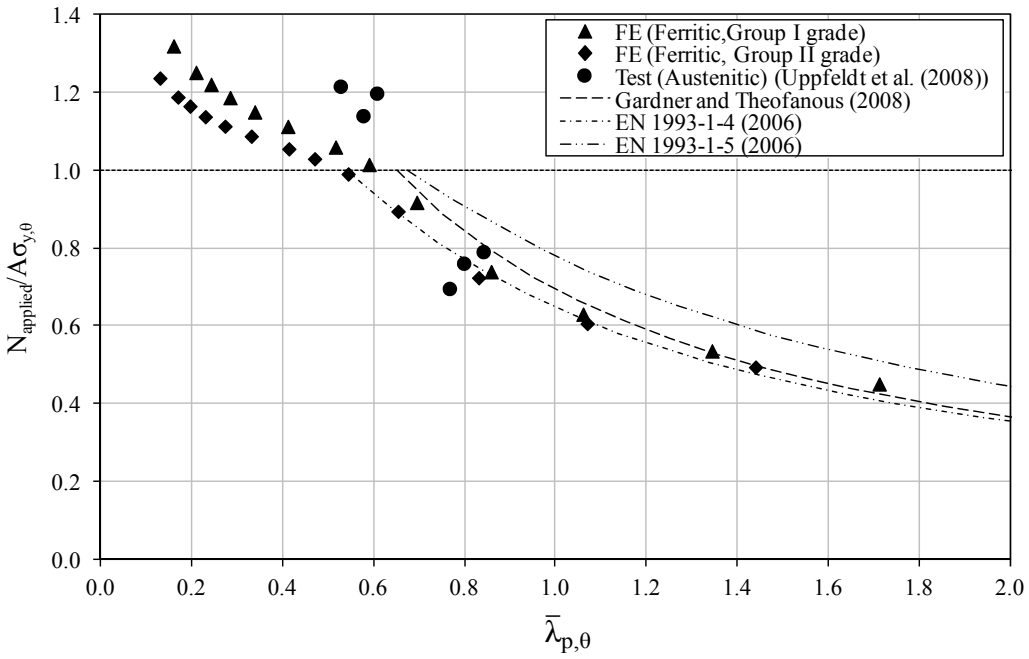

Fig. 3.13. Comparison of the existing effective width formulae with FE and test results

Table 3.9. Proposed cross-section design method

Cross-section classification limits	Effective width formula
Gardner and Theofanous [25] limits with: $\varepsilon_\theta=\left[\left(\frac{235}{f_y}\frac{E}{210000}\right)\left(\frac{k_{E,\theta}}{k_{2,\theta}}\right)\right]^{0.5}$ Class 1 & 2 sections at room temperature $\varepsilon_\theta=\left[\left(\frac{235}{f_y}\frac{E}{210000}\right)\left(\frac{k_{E,\theta}}{k_{0.2,\theta}}\right)\right]^{0.5}$ Class 3 & 4 sections at room temperature	Gardner and Theofanous [25] formula with: $\bar{\lambda}_{p,\theta}=\frac{\bar{b}/t}{28.4\varepsilon_\theta\sqrt{k_\sigma}}$

Tables 3.10 and 3.11 provide a comparison between the FE results for the beams and columns with the predictions from EN 1993-1-2 [1], Ng and Gardner [5] and the proposed method – in terms of the predicted resistance over the FE results. Since the modelled beams were subjected to fire on 3 sides only, non-uniform temperature distribution across the cross-section exists, whilst the temperature is uniform along the length. Hence, the design resistance has been calculated on the basis of the average temperature of the cross-section at failure.

Table 3.10 Comparison of the design methods for ferritic stainless steel columns

	EN 1993-1 & EN 1993-1-4	Ng and Gardner (2007)	Proposed
Mean	0.824	0.945	0.979
COV	0.074	0.067	0.094

Table 3.11 Comparison of the design methods for ferritic stainless steel columns

	EN 1993-1 & EN 1993-1-4	Ng and Gardner (2007)	Proposed
Mean	0.919	0.969	1.007
COV	0.086	0.063	0.059

3.4.3 Compression members

Existing design rules for elevated temperature resistance of compression members provided in EN 1993-1-2 [1] and its modified versions proposed by Ng and Gardner [5] , Uppfeldt et al. [23] and Lopes et al. [22] are reviewed and assessed in this section. Based on EN 1993-1-2, the design fire resistance of stainless steel structures, assuming a uniform temperature distribution, is based on the room temperature design resistance, supplied in EN 1993-1-4 [20], modified to take account of the mechanical properties at elevated temperature and with a revised buckling curve. The fire buckling curve in EN 1993-1-2 is of the same general form as the room temperature buckling curve with the exception of exhibiting no plateau (i.e. $\bar{\lambda}_0 = 0$), including a yield strength dependent imperfection factor $\alpha = 0.65\sqrt{(235/f_y)}$ and defining the elevated temperature member non-dimensional slenderness, $\bar{\lambda}_\theta$. Ng and Gardner [5] proposed a revised buckling curve with the plateau length $\bar{\lambda}_0 = 0.2$ and the imperfection factor taken as $\alpha = 0.55$. Uppfeldt et al. [23] proposed to use the same buckling curve as room temperature, with $\bar{\lambda}_0 = 0.4$ and $\alpha = 0.49$ (for hollow sections), for elevated temperature design, with the plateau length changing as a function of temperature. Based on their numerical study on welded I-section columns in fire, Lopes et al. [22] modified the EN 1993-1-2 buckling curve such that it provides a good fit to the generated data. The imperfection factor α is defined as a function of temperature, resulting in different buckling curves for different temperatures. Table 3.12 provides a summary of the above mentioned guidelines for the fire design of stainless steel compression members.

Table 3.12: Elevated temperature member buckling design approaches from current design guidance

Design standard	Member compression resistance
EN 1993-1-4 & EN 1993-1-2. [1, 20]	For Class 1, 2 & 3 cross-sections: $N_{b,fi,t,Rd} = \frac{\chi_{fi} A k_{2,\theta} f_y}{\gamma_{M,fi}}$ For Class 4 sections: $N_{b,fi,t,Rd} = \frac{\chi_{fi} A_{eff} k_{0.2,\theta} f_y}{\gamma_{M,fi}}$ where, $\chi_{fi} = \frac{1}{\phi_\theta + \sqrt{\left(\phi_\theta^2 - \bar{\lambda}_\theta^2\right)}}$ but ≤ 1.0 $\phi_\theta = 0.5\left[1 + 0.65\sqrt{(235/f_y)}\,\bar{\lambda}_\theta + \bar{\lambda}_\theta^2\right]$ $\bar{\lambda}_\theta = \bar{\lambda}\left[k_{2,\theta} \text{ or } k_{0.2,\theta}/k_{E,\theta}\right]^{0.5}$
Euro Inox/SCI Design Manual. [21]	For Class 1, 2 & 3 cross-sections: $N_{b,fi,t,Rd} = \frac{\chi_{fi} A k_{0.2,\theta} f_y}{\gamma_{M,fi}}$ For Class 4 sections: $N_{b,fi,t,Rd} = \frac{\chi_{fi} A_{eff} k_{0.2,\theta} f_y}{\gamma_{M,fi}}$ where, $\chi_{fi} = \frac{1}{\phi_\theta + \sqrt{\left(\phi_\theta^2 - \bar{\lambda}_\theta^2\right)}}$ but ≤ 1.0 $\phi_\theta = 0.5\left[1 + \alpha(\bar{\lambda}_\theta - \bar{\lambda}_0) + \bar{\lambda}_\theta^2\right]$, $\alpha = 0.49$ and $\bar{\lambda}_0 = 0.4$ $\bar{\lambda}_\theta = \bar{\lambda}\left[k_{0.2,\theta}/k_{E,\theta}\right]^{0.5}$ for all cross-section classes

Ng and Gardner. [5]	For Class 1, 2 cross-sections: $N_{b,fi,t,Rd} = \frac{\chi_{fi} A k_{2,\theta} f_y}{\gamma_{M,fi}}$ For Class 3 cross-sections: $N_{b,fi,t,Rd} = \frac{\chi_{fi} A k_{0.2,\theta} f_y}{\gamma_{M,fi}}$ For Class 4 sections: $N_{b,fi,t,Rd} = \frac{\chi_{fi} A_{eff} k_{0.2,\theta} f_y}{\gamma_{M,fi}}$ where, $\chi_{fi} = \frac{1}{\phi_\theta + \sqrt{\left(\phi_\theta^2 - \bar{\lambda}_\theta^2\right)}}$ but ≤ 1.0 $\phi_\theta = 0.5\left[1+\alpha\left(\bar{\lambda}_\theta - \bar{\lambda}_0\right) + \bar{\lambda}_\theta^2\right]$, $\alpha = 0.55$ and $\bar{\lambda}_0 = 0.2$ $\bar{\lambda}_\theta = \bar{\lambda}\left[k_{2,\theta} \text{or } k_{0.2.\theta}/k_{E,\theta}\right]^{0.5}$
Lopes et al. [22]	For Class 1, 2 & 3 cross-sections: $N_{b,fi,t,Rd} = \frac{\chi_{fi} A k_{2,\theta} f_y}{\gamma_{M,fi}}$ For Class 4 sections: $N_{b,fi,t,Rd} = \frac{\chi_{fi} A_{eff} k_{0.2,\theta} f_y}{\gamma_{M,fi}}$ where, $\chi_{fi} = \frac{1}{\phi_\theta + \sqrt{\left(\phi_\theta^2 - \beta\bar{\lambda}_\theta^2\right)}}$ but ≤ 1.0 $\phi_\theta = 0.5\left[1+\alpha\bar{\lambda}_\theta+\beta\bar{\lambda}_\theta^2\right]$ $\beta = 1.0$ and 1.5 for major axis and minor axis buckling, respectively and $\alpha = \eta\varepsilon$. $\alpha = \eta\left[\frac{235}{f_y}\frac{E}{210000}\right]^{0.5}\left[\frac{k_{E,\theta}}{k_{2,\theta} \text{ or } k_{0.2,\theta}}\right]^{0.5}$ $\eta = 1.3$ $\bar{\lambda}_\theta = \bar{\lambda}\left[k_{2,\theta} \text{or } k_{0.2,\theta}/k_{E,\theta}\right]^{0.5}$

Uppfeldt et al. [23]	For Class 1 & 2 cross-sections: $N_{b,fi,t,Rd} = \frac{\chi_{fi} A k_{2,\theta} f_y}{\gamma_{M,fi}}$ For Class 3 sections: $N_{b,fi,t,Rd} = \frac{\chi_{fi} A k_{0.2,\theta} f_y}{\gamma_{M,fi}}$ For Class 4 sections: $N_{b,fi,t,Rd} = \frac{\chi_{fi} A_{eff} k_{0.2,\theta} f_y}{\gamma_{M,fi}}$ where, $\chi_{fi} = \frac{1}{\phi_\theta + \sqrt{\left(\phi_\theta^2 - \bar{\lambda}_\theta^2\right)}}$ but ≤ 1.0 $\phi_\theta = 0.5\left[1+\alpha(\bar{\lambda}_\theta - \bar{\lambda}_{0,\theta}) + \bar{\lambda}_\theta^2\right]$ $\bar{\lambda}_{0,\theta} = \bar{\lambda}_0 \left(\frac{k_{2,\theta} \text{ or } k_{0.2,\theta}}{k_{E,\theta}}\right)^{0.5}$ $\alpha = 0.49$ and $\bar{\lambda}_0 = 0.4$ $\bar{\lambda}_\theta = \bar{\lambda}\left[k_{2,\theta} \textit{ or } k_{0.2,\theta}/k_{E,\theta}\right]^{0.5}$

Figures 3.14-3.18 compare the above mentioned buckling curves with an average plateau length of 0.285 for the investigated specimens for the Uppfeldt et al. [23] model, and an average failure temperature of 640 °C for the Lopes et al. [22] model with the test and parametric study results, where the applied load, normalised by the appropriate elevated temperature yield load is plotted against the elevated temperature member slenderness. The buckling curves proposed by Lopes et al. (2010) are considerably lower than other studies. A preliminary study into the effect of section type and presence of residual stresses has shown that, the buckling performance of welded I-sections, for which Lopes et al. recommendations were developed, is distinctly different from that of cold-formed box sections.

A revised buckling curve, with the general form of the room temperature buckling curve of EN 1993-1-4, but, with imperfection parameter $\alpha = 0.49$ and limiting slenderness $\bar{\lambda}_0 = 0.2$ is proposed for cold-formed SHS/RHS members. The proposed buckling curve, which has also been shown to work well for room temperature design of cold-formed ferritic stainless steel column tubular columns [27], provides an improved representation of the fire resistance of ferritic stainless steel columns at elevated temperatures.

The definition of member slenderness at elevated temperature, in terms of the room temperature member slenderness, provided by the design proposals in Table 3.12 is not in line with the cross-section classification at elevated temperature. Since the cross-section classification may change at elevated temperatures, which in turn changes the cross-section area from gross to effective, or vice versa, the member slenderness is redefined appropriately, as given by Eq. (3.9).

$$\bar{\lambda}_\theta = \sqrt{A_\theta f_{y,\theta} / N_{cr,\theta}} \tag{3.9}$$

where, $A_\theta = A_{gross}$ for sections which are Class1, 2 and 3 at elevated temperature and $A_\theta = A_{eff}$ for sections which are Class 4 at elevated temperature.

Considering the design proposals made at both cross-section level and member level, the FE and test results are plotted in Figure 3.19 with the revised buckling curve also depicted. Numerical comparisons in terms of the mean and the coefficient of variation (COV) of the predicted resistance over the FE and test results are also provided in Table 3.13.

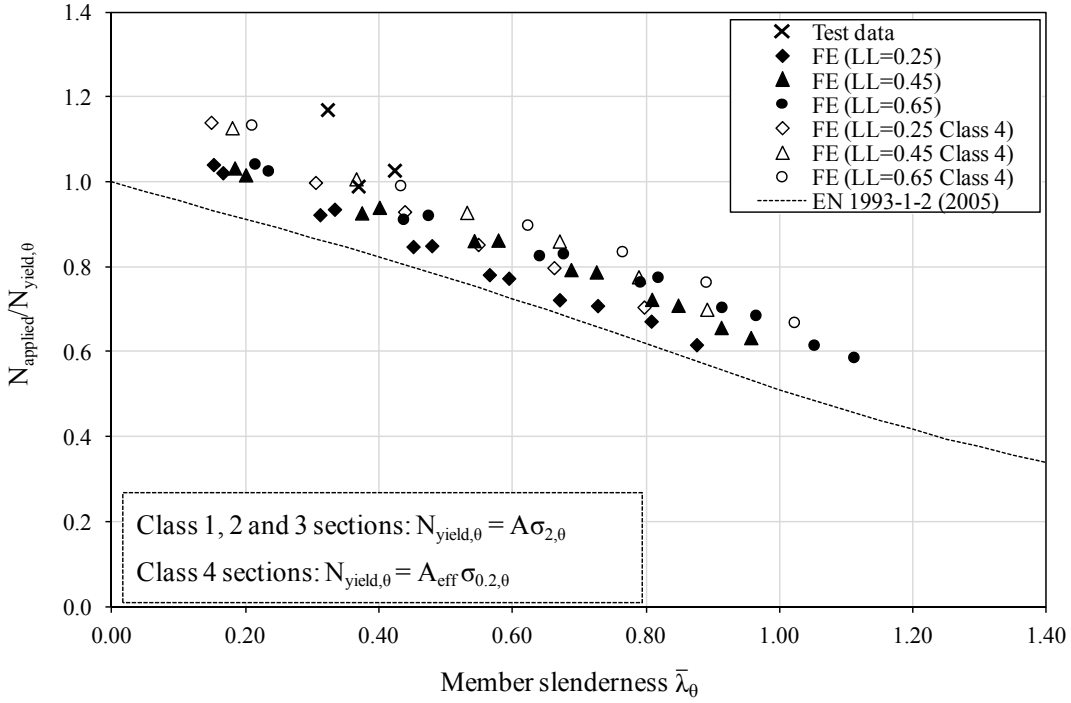

Fig. 3.14 Comparison of FE and test results with EN 1993-1-2 [1] provisions.

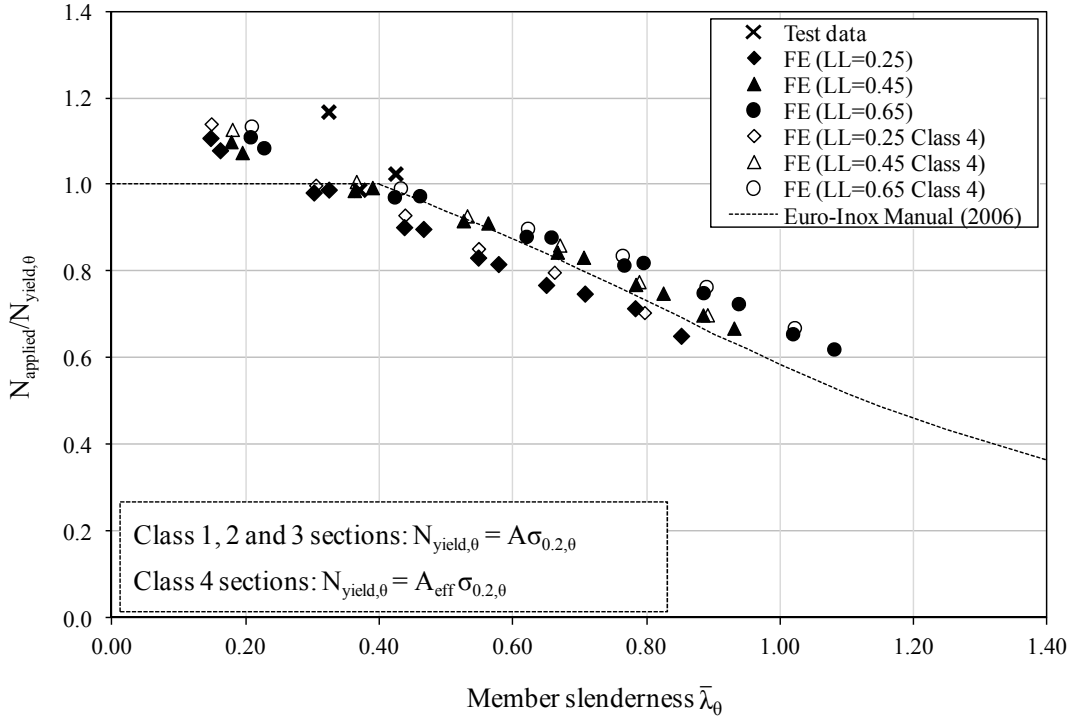

Fig. 3.15 Comparison of FE and test results with Euro Inox/SCI design manual [21] provisions.

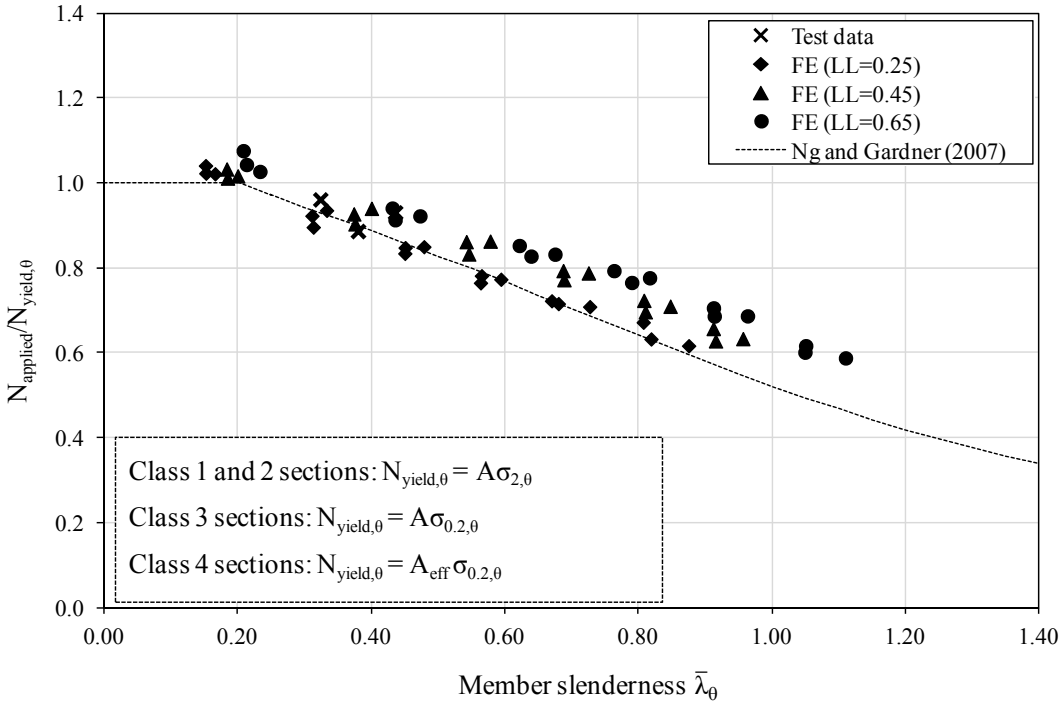

Fig. 3.16 Comparison of FE and test results with Ng and Gardner [5] proposal.

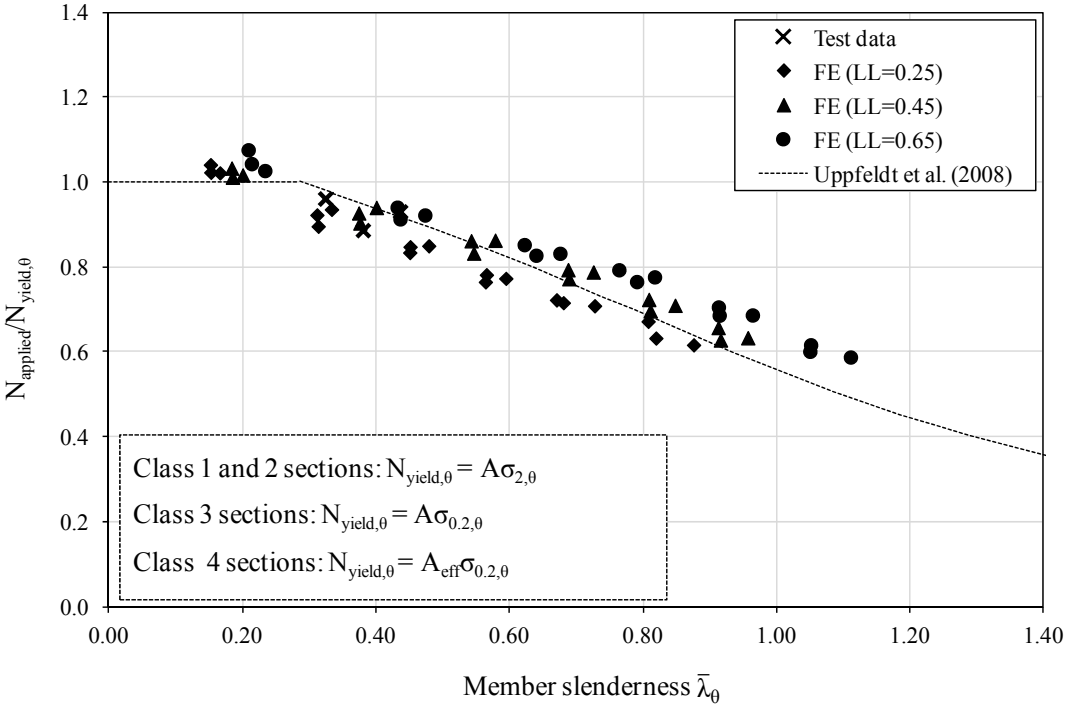

Fig. 3.17 Comparison of FE and test results with Uppfeldt et al. [23] proposal.

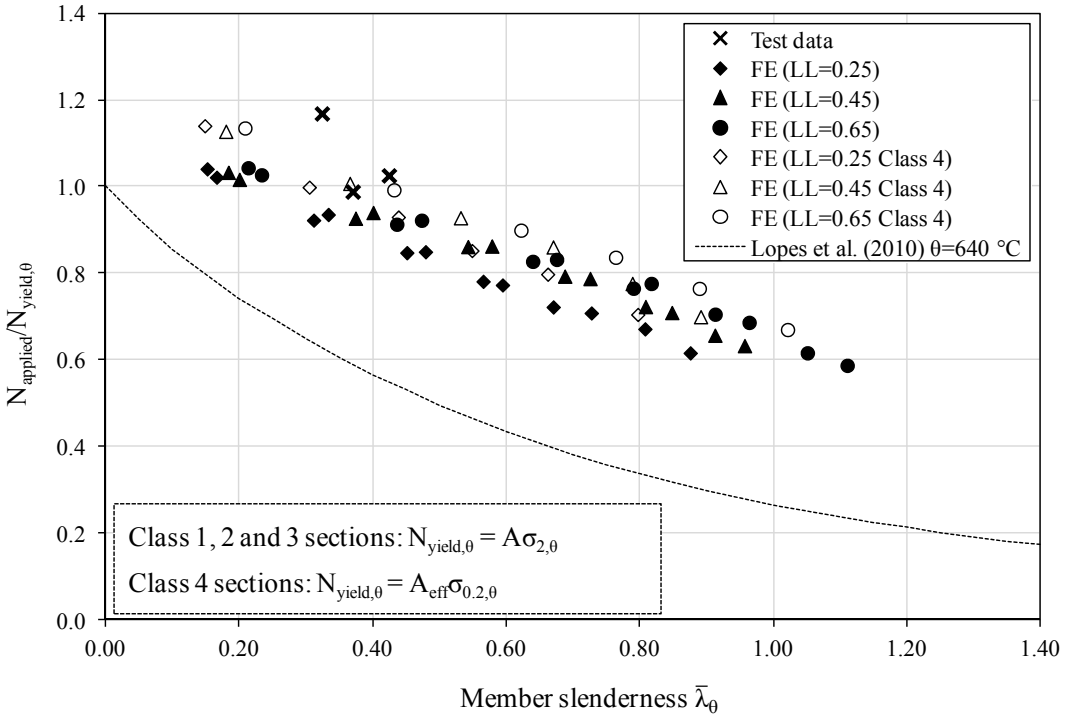

Fig. 3.18 Comparison of FE and test results with Lopes et al. [22] proposal.

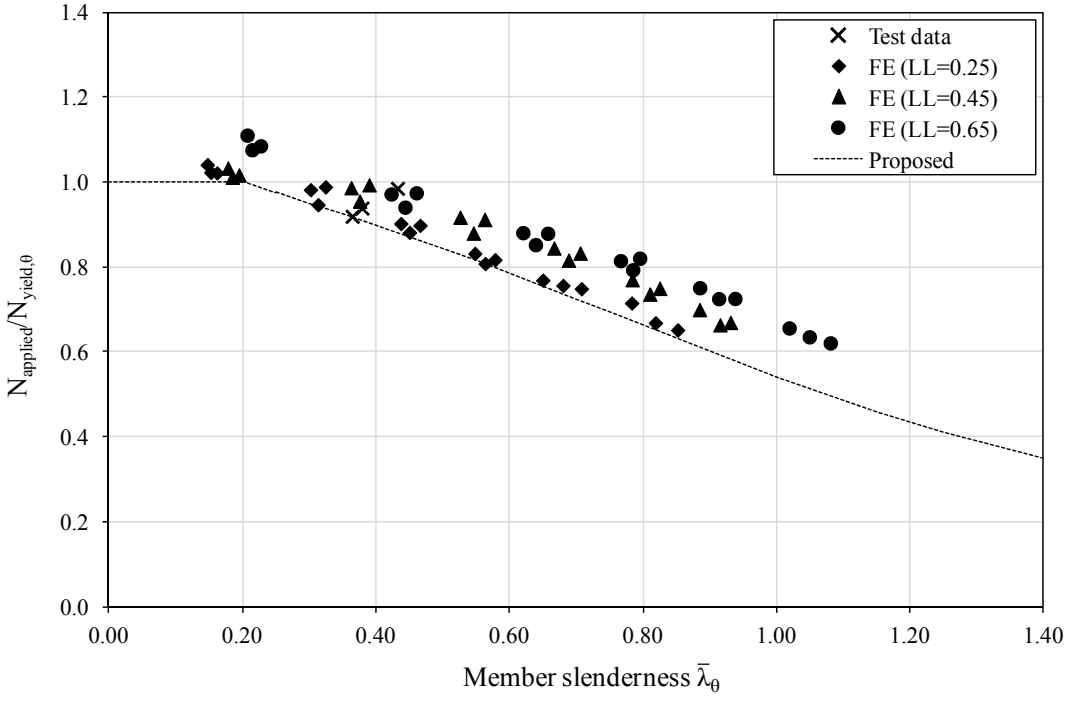

Fig. 3.19 Comparison of FE and test results with the proposed method.

Table 3.11 Comparison of FE and test results with existing design guidance and proposed approach

	EN 1993 -1-2	Euro Inox Design Manual	Ng and Gardner (2007)	Uppfeldt et al. (2008)	Lopes et al. (2012)	Proposed
Mean	0.849	0.969	0.931	0.981	0.595	0.915
COV	0.066	0.071	0.074	0.062	0.177	0.066

4 References

[1] EN 1993-1-2. Eurocode 3: Design of steel structures - Part 1-2: General rules - Structural fire design, European Committee for Standardization (CEN), Brussels, 2005.

[2] L. Gardner, N.R. Baddoo, Fire testing and design of stainless steel structures, Journal of Constructional Steel Research, 62 (2006) 532-543.

[3] T. Ala-Outinen, T. Oksanen, Stainless steel compression members exposed to fire. Research notes 1864, Finland. VTT building technology,, 1997.

[4] ABAQUS - Version 6.10-1, Dassault Systèmes Simulia Corp, USA, 2010.

[5] K. Ng, L. Gardner, Buckling of stainless steel columns and beams in fire, Engineering Structures, 29 (2007) 717-730.

[6] E.C.-Y. To, B. Young, Performance of cold-formed stainless steel tubular columns at elevated temperatures, Engineering Structures, 30 (2008) 2012-2021.

[7] L. Gardner, A. Insausti, K. Ng, M. Ashraf, Elevated temperature material properties of stainless steel alloys, Journal of Constructional Steel Research, 66 (2010) 634-647.

[8] B. Rossi, S. Afshan, L. Gardner, Strength enhancements in cold-formed structural sections — Part II: Predictive models, Journal of Constructional Steel Research, 83 (2013) 189-196.

[9] R.B. Cruise, L. Gardner, Strength enhancements induced during cold forming of stainless steel sections, Journal of Constructional Steel Research, 64 (2008) 1310-1316.

[10] J. Chen, B. Young, Stress–strain curves for stainless steel at elevated temperatures, Engineering Structures, 28 (2006) 229-239.

[11] EN 10088-1. Stainless steels - Part 1: List of stainless steels, European Committee for Standardization (CEN), Brussels, 2005.

[12] S. Gmbh, Stahldat SX.[online] Available at: http://www.stahldaten.de [Accessed: 12 November 2012]. 2011.

[13] Aperam, Technical data sheets and Surface finishes data sheets. [online] Available at: http://www.aperam.com/europe/news-publications/documentation/technical-data-sheets-2 [Accessed: 10 March 2013]. (2013).

[14] M. Ashraf, L. Gardner, D.A. Nethercot, Finite element modelling of structural stainless steel cross-sections, Thin-walled structures, 44 (2006) 1048-1062.

[15] R. Cruise, L. Gardner, Residual stress analysis of structural stainless steel sections, Journal of Constructional Steel Research, 64 (2008) 352-366.

[16] K. Rasmussen, G. Hancock, Design of cold-formed stainless steel tubular members. I: Columns, Journal of Structural Engineering (ASCE), 119 (1993) 2349-2367.

[17] EN 1363-1. Fire resistance tests - Part 1: General requirements., European Committee for Standardization (CEN). Brussels, 1999

[18] EN 1991-1-2. Eurocode 1: Actions on structures - Part 1-2: General actions - Actions on structures exposed to fire. , European Committee for Standardization (CEN), Brussels, 2002.

[19] 1090-2. Execution of steel structures and aluminium structures Part 2: Technical requirements for steel structures., European Committee for Standardization (CEN), Brussels, 2008.

[20] EN 1993-1-4. Eurocode 3: Design of steel structures - Part 1-4: General rules - Supplementary rules for stainless steels, European Committee for Standardization (CEN), Brussels, 2006.

[21] Euro Inox/SCI. Design manual for structural stainless steel., Third Edition ed., Euro Inox and the Steel Construction Institute., 2006.

[22] N. Lopes, P.V. Real, L.S. da Silva, J.-M. Franssen, Axially loaded stainless steel columns in case of fire, Journal of Structural Fire Engineering, 1 (2010) 43-60.

[23] B. Uppfeldt, T. Ala Outinen, M. Veljkovic, A design model for stainless steel box columns in fire, Journal of Constructional Steel Research, 64 (2008) 1294-1301.

[24] EN 1993-1-1. Eurocode 3: Design of steel structures - Part 1-1: General rules and rules for buildings, European Committee for standardization (CEN), Brussels, 2005.

[25] L. Gardner, M. Theofanous, Discrete and continuous treatment of local buckling in stainless steel elements, Journal of Constructional Steel Research, 64 (2008) 1207-1216.

[26] EN 1993-1-5. Eurocode 3: Design of steel structures - Part 1-5: Plated structural elements, European Committee for standardization (CEN), Brussels, 2006.

[27] S. Afshan, L. Gardner, Experimental study of cold-formed ferritic stainless steel hollow sections, Journal of Structural Engineering (ASCE), 139 (2013) 717-728.